

1 **A universal hippocampal memory code across animals and environments**

2

3 Hannah S Wirtshafter^{1*}, Sara A Solla¹, John F Disterhoft¹

4

5

6

7

8

9 *Lead contact: hsw@northwestern.edu (HSW)

10

11

12

13

14

15

16

17 1. Department of Neuroscience, Northwestern University Feinberg School of Medicine, Chicago,

18 IL, USA.

19

20 **How learning is affected by context is a fundamental question of neuroscience, as the ability to**
21 **generalize learning to different contexts is necessary for navigating the world. An example of**
22 **swift contextual generalization is observed in conditioning tasks, where performance is quickly**
23 **generalized from one context to another. A key question in identifying the neural substrate**
24 **underlying this ability is how the hippocampus (HPC) represents task-related stimuli across**
25 **different environments, given that HPC cells exhibit place-specific activity that changes across**
26 **contexts (remapping). In this study, we used calcium imaging to monitor hippocampal neuron**
27 **activity as rats performed a conditioning task across multiple spatial contexts. We investigated**
28 **whether hippocampal cells, which encode both spatial locations (place cells) and task-related**
29 **information, could maintain their task representation even when their spatial encoding**
30 **remapped in a new spatial context. To assess the consistency of task representations, we used**
31 **advanced dimensionality reduction techniques combined with machine learning to develop**
32 **manifold representations of population level HPC activity. The results showed that task-related**
33 **neural representations remained stable even as place cell representations of spatial context**
34 **changed, thus demonstrating similar embedding geometries of neural representations of the**
35 **task across different spatial contexts. Notably, these patterns were not only consistent within**
36 **the same animal across different contexts but also significantly similar across different animals,**
37 **suggesting a standardized neural encoding or 'neural syntax' in the hippocampus. These**
38 **findings bridge a critical gap between memory and navigation research, revealing how the**
39 **hippocampus maintains cognitive consistency across different spatial environments. These**
40 **findings also suggest that hippocampal function is governed by a neural framework shared**
41 **between animals, an observation that may have broad implications for understanding memory,**
42 **learning, and related cognitive processes. Looking ahead, this work opens new avenues for**
43 **exploring the fundamental principles underlying hippocampal encoding strategies.**

44 **Introduction**

45 How can learning can be generalized across contexts as well as remaining localized to one
46 context? This question is fundamental to both neuroscience and philosophy¹⁻⁴. Deficits in
47 generalization or inappropriate generalization are hallmarks of many disorders, including
48 autism^{5,6}, schizophrenia^{7,8}, and post-traumatic stress disorder^{9,10}. In spite of their importance,
49 many questions related to generalization remain to be answered.

50
51 The hippocampus (HPC) is important for learning, memory, and navigation, and damage to
52 this region can disrupt contextual learning¹¹⁻¹⁷. Many aspects of context, including an animal's
53 spatial location and the presence of local and distal cues, can be represented by 'place cells' in
54 the HPC¹⁸⁻²². The activity of many HPC cells therefore changes drastically in different
55 environments (i.e. place cells remap), even when a task can be generalized across these different
56 contexts²³⁻²⁵. A major open question is if and how representations of task-relevant stimuli, which
57 are also found in the HPC²⁶⁻³¹, can be maintained against the background of remapped place
58 cells. A further question is whether different animals solve this problem using the same, or
59 similar, neural strategies.

60
61 Until recently, the neural mechanisms behind contextual learning have been challenging to
62 investigate due to the need for tracking large numbers of cells across various environments and
63 learning stages— tasks which were unachievable prior to the development of calcium imaging³²⁻
64 ³⁷. The use of calcium imaging in this study has allowed for a detailed exploration of
65 hippocampal neuron dynamics, bridging previous gaps between studies of hippocampal

66 cognitive maps and the hippocampal bases of memory and learning. The traditional separation
67 between memory and navigation fields of HPC research is thus in the process of narrowing^{38,39}.

68 This research addresses two fundamental questions of learning and memory. The first
69 question pertains to the persistence of learning across varying contexts. The modulation of
70 hippocampal cells by spatial variables results in substantial changes to cell activity in different
71 environments^{24,25,40,41}; how can conditioning-related neural representations remain stable amid
72 such remapping? The second question is the extent to which neural representations in the
73 hippocampus are invariant and consistent, not only within an individual across diverse contexts,
74 but across different individuals; is there a standardized neural encoding or 'neural syntax' in the
75 for learning and memory in the hippocampus? A commonality of encoding across animals would
76 imply that the functionality of the HPC is informed not solely by individual experiences but also
77 by a standardized framework of neural algorithms. Such a finding would provide key insights
78 into the underlying neural mechanisms that govern learning and memory, helping to identify
79 specific brain circuits and algorithms that drive behavior.

80 To answer these questions, we trained rats on an HPC-dependent conditioning task which is
81 rapidly generalized between spatial contexts^{42,43}. We examined the same task in disparate
82 contexts and looked for changes in a representation of spatial location provided by a population
83 of place cells while the representation of the task features remains unchanged. We found that the
84 representations of the conditioning task were maintained as the animal generalized learning from
85 one environment to another, even as the representation of place changed. Surprisingly, we also
86 found that the neural representation of the task was consistent across animals.

87

88 This study demonstrates that despite the well-known phenomenon of place cell
89 remapping^{24,25,40,41}, there exists a stable population-level neural representation of task features
90 that persists across diverse environments. These representations also show consistency across
91 different individuals, indicating a standardized neural encoding or 'neural syntax' for the
92 conditioning task within the hippocampus. This novel finding suggests the existence of a
93 universal coding mechanism for associative learning in the hippocampus, a principle that could
94 reorient our approach to studying memory and could challenge our current understanding of
95 cognitive processes.

96

97

98

99 **Results**

100 We trained a cohort of 5 freely moving rats in a conditioning task in one of two distinct
101 environments, labeled A and B; the rats had been previously familiarized with the environment
102 by the time the training began (Fig. 1a, Fig. S1). Environment A was an unscented rectangular
103 enclosure with wire floor and walls, and white lighting; environment B was a scented ovalar
104 enclosure with white solid floor and walls, and red lighting (Fig. 1b). Both environments were
105 located at the same spot in the room relative to external cues (see Methods); animals could see
106 external cues out of the top of both environments, as well as out of the sides of environment A
107 (animals also reared often, allowing them to see out of the sides of environment B). During
108 training sessions, we recorded cellular activity in the hippocampal CA1 region via miniscopes,
109 using Gcamp8m for calcium imaging (CaImg). To perform data analysis, we used both calcium
110 events and calcium traces (see Methods), as indicated when applicable.

111

112 *Animals easily transfer a conditioning task across environments*

113 During the initial phase of our study, freely-moving rats (Fig. 1b) underwent training for
114 trace eyeblink conditioning (tEBC) (Fig. S2), a hippocampus-dependent classical conditioning
115 task that serves as a robust model for associative memory formation⁴⁴⁻⁴⁷. This paradigm involves
116 presenting a 250ms conditioned stimulus (CS, in the form of a tone) followed by a 500ms trace
117 interval, followed by the 100ms presentation of an unconditioned stimulus (US, an eyelid shock)
118 (Fig. 1c). Both shock and blinking were recorded with wires inserted into the muscle of the
119 eyelid (see Methods). As rats were trained, they exhibited a conditioned blink (CR) to the tone.
120 Animals were considered to have learned the task after reaching criterion (70% CRs in 50 trials)
121 on three consecutive training sessions (termed ‘criterion sessions’) or when the previous four

122 training sessions averaged over 70% (in this instance, only the final three of those sessions were
123 considered ‘criterion sessions’) (Fig. 1d). There was substantial variability in the number of
124 sessions it took to learn the task, for an average of 20 ± 4.2 training sessions (note: number of
125 sessions always includes criterion sessions). The two rats that learned the fastest reached
126 criterion in 14 sessions, and the rat that learned the slowest reached criterion after 24 sessions
127 (Fig. S2). After reaching criterion, the rats were introduced to environment B, where their ability
128 to perform tEBC was assessed over a two-day period (one session per day). Comparative
129 analysis revealed no significant difference in performance (measured in % CRs) between the
130 criterion sessions in environment A and the testing phase in environment B (mean in
131 environment A criterion sessions was 74.75 ± 6.49 , mean in environment B test sessions was
132 77.70 ± 11.68 , two tailed t-test(24) = -0.83, $p > 0.05$) (Fig. 1d), indicating the successful transfer of
133 tEBC learning to a new environment.

134

135 Calcium imaging (CaImg) enabled the longitudinal monitoring of the same hippocampal
136 cells over multiple sessions in both environments. For criterion and testing sessions, we observed
137 an average of 459.85 ± 265.31 cells per session per animal, with no significant difference between
138 the number of cells recorded in environment A and environment B (two-tailed t-test(24) = -0.56,
139 $p > 0.05$) On average, 132 ± 95 cells were present in both the last criterion session in A and the first
140 testing session in B. This was not a significantly different numbers of cells that were present, on
141 average, in both the semi-final session in A, session A(n-1), and the final session in A, session
142 A(n) (155 ± 115 cells).

143

144 ***Hippocampal place cell representations differ across environments***

145 To identify place cells, we compared actual mutual information (MI) to MI computed
146 after bootstrapping circularly shifted position data 500 times. A cell was deemed a place cell if
147 its MI was above the 95th percentile of null provided by the bootstrapped MI scores. Using this
148 95% cutoff, on average, $9.3\% \pm 4.2\%$ of cells across criterion sessions in A and testing sessions in
149 B qualified as place cells. There was not a significant difference between the percent of cells that
150 qualified as place cells in environment A and environment B (average in environment A was
151 $8.1\% \pm 3.3\%$, average in environment B was $11.1\% \pm 4.9\%$, two-tailed t-test $t(23) = -1.9$, $p > 0.05$)
152 (Fig. 2a, Fig. S3). The average mutual information scores across all criterion and testing sessions
153 was 1.08 ± 0.18 , with no difference in average MI between environments (environment A mean
154 MI was 1.08 ± 0.17 , environment B mean MI was 1.08 ± 0.21 , two-tailed t-test $t(4805) = -0.5$,
155 $p > 0.05$). (See methods for more detailed analysis).

156

157 Our analysis revealed that individual hippocampal (HPC) cells exhibited distinct spatial
158 representations for environments A and B, altering their configurations of place cells and place
159 fields relative to distal cues — a process known as 'place cell remapping' (Fig. 2b). We
160 confirmed this remapping through several approaches. First, we quantified the shift in the
161 location of highest calcium event rate (putative place field centers) by comparing their distances
162 on the last two criterion sessions in environment A (sessions A(n-1) and A(n)) to the shift
163 observed when transitioning from environment A on session n to environment B on session 1
164 (the centers of both environments were aligned, see methods). The data indicated a significantly
165 greater change in these putative place field centers when the animals transitioned from A to B
166 than when remaining within environment A (medians tested with Wilcoxon rank sum test
167 $p = 0.002$, means tested with double sided t-test $t(1430) = -2.5$, $p = 0.01$, distributions tested with

168 two-sample Kolmogorov-Smirnov (KS) test, $p=3.6 \times 10^{-4}$) (Fig. 2c). Second, to compensate for
169 any differences in environment size, we also compared the distances between field centers to the
170 distances expected if all centers were shuffled 100 times, and found that the median distance
171 between field centers when comparing session A(n) to session A(n-1) was less than all median
172 shuffled values ($p=0$), while the median distance between field centers when comparing session
173 A(n) to session B(1) was greater or equal than 56% of shuffled values ($p=0.56$) (Fig. 2d). Third,
174 accounting for the fact that cells may have multiple place fields, we computed the population
175 vector correlation (PVC^{40,48,49}, see methods) using calcium events for sessions A(n-1), A(n), and
176 B(1). When using cells that appeared in both sessions A(n-1) and A(n), we found a significant
177 positive correlation when computing the PVC for these two sessions ($p = 0.0023$, $r = 0.11$).
178 Conversely, when using cells that appeared in both sessions A(n) and B(1), we found no
179 correlation ($p>0.05$, $r=-0.04$). This result indicates significantly similar calcium event patterns
180 between sessions A(n-1) and session A(n), with no significant similarity in patterns between
181 session A(n) and B(1). (Fig. 2e).

182

183 We then used a machine learning algorithm to determine the variation in neural
184 embeddings between environments A and B. To do this, we applied the CEBRA algorithm⁵⁰ to
185 calcium trace imaging data labelled with spatial coordinates from environment A, session A(n)
186 (all were trained on 75% of data with 25% held out for verification). The choice of CEBRA was
187 motivated by its efficacy and interpretability in decoding neural activity patterns when compared
188 to alternative methods such as PCA⁵¹ and Isomap⁵² (see Methods for additional details). We then
189 tested this model's ability to decode the animals' position in environment A and environment B
190 when applied to neural data not used for training. The results showed that the model, when run

191 500 times, predicted the positions in session A(n-1) with significantly greater accuracy than what
192 would be expected by chance; the null was constructed as determined when compared to a model
193 trained on shuffled position data and also run 500x. (All double sided t-tests, for each rat: rat1:
194 $t(998)=-34.3$ $p=5.0*10^{-171}$, rat2: $t(998)=-72.5$ $p=0$, rat3: $t(998)=-1.96$ $p=0.05$, rat4: $t(998)=-53.7$
195 $p=2.6*10^{-299}$, rat5: $t(998)=-20.0$ $p=4.1*10^{-75}$) (Fig. 3a-b). In contrast, when a model trained on
196 data from A(n) was applied to environment B, the model's predictions were significantly below
197 the accuracy of a model trained on shuffled position data, implying that the place cell coding
198 across environments A and B are actually more different than would be expected by chance (all
199 double sided t-tests, for each rat: rat1: $t(998):84.1$ $p=0$, rat2: $t(998):18.8$ $p=7.4*10^{-68}$, rat3:
200 $t(998)=74.7$ $p=0$, rat4: $t(998):13.1$ $p=2.0*10^{-36}$, rat5: $t(998):154.4$ $p=0$) (Fig. 3c-d). Collectively,
201 these findings suggest a significant remapping of place cells when transitioning between
202 environments, and also that the neural embeddings for place coding in individual rats change
203 when the animal switches contexts.

204

205 ***The hippocampus represents the conditioning task in both environments, and representations***
206 ***of the conditioning task are not spatial representations***

207

208 We then investigated whether conditioning related data was represented equally in both
209 environments A and B. It was obvious on visual inspection that individual cells varied their
210 calcium event rate (Fig. 4a) and calcium trace (Fig. 4b) during the conditioning periods. To
211 quantify this variation, we devised the metric 'CSUS mutual information' (CSUS-MI), analogous
212 to spatial mutual information; this enabled us to assess the extent of task-related information
213 captured by the calcium activity of each cell. We calculated the CSUS-MI for each cell and

214 benchmarked it against a control distribution generated by shuffling CS and US periods and
215 recalculating the MI 500 times. Using calcium event data, we found that $10.7 \pm 4.9\%$ of cells held
216 significant CSUS information related to whether the animal was in a CS or US period (termed
217 CSUS-MI2 as the conditioning period was divided into 2 bins; see Methods) (Fig. S4a). An even
218 stronger relationship was noted if using calcium traces: 19.9 ± 8.2 percent of cells contained
219 significant information related to whether the animal was in a CS or US period (Fig. S4a).
220 Importantly, neither of these MI metrics were significantly different between environments A
221 and B (double sided t-tests, using calcium events, $t(23)=0.48$, $p>0.05$, using calcium traces,
222 $t(23)=-0.52$, $p>0.05$).

223 We then extended this analysis to determine if calcium events or traces of individual cells
224 contained information about what temporal segment portion of the conditioning task the animal
225 was in. To do this, we divided the CSUS period into 5 equal sized bins, computed CSUS-MI
226 using these bins (termed CSUS-MI5, see methods), then compared these mutual information
227 values to the controls provided by shuffled data. Using calcium event data, we found that
228 $15.5 \pm 7.8\%$ of cells contained this information, compared to $10.0 \pm 7.8\%$ of cells when we
229 calculated the MI using trace information (Fig. S4b). Again, neither of these mutual information
230 metrics were significantly different between environments A and B (double sided t-tests, using
231 calcium event data, $t(23)=-0.32$, using calcium trace data, $t(23)=-1.1$, $p>0.05$). There was not a
232 significant difference in CSUS-MI2 values when comparing values in session A(n) to session
233 A(n-1), versus comparing values in session A(n) to session B(1) (Wilcoxon rank sum test
234 $p>0.05$, double sided t-test, $t(1431)=0.86$, $p>0.05$). In contrast, there was a small but significant
235 difference in CSUS-MI5 when comparing session A(n) to session A(n-1) versus comparing A(n)
236 to session B(1) (Wilcoxon rank sum test $p=0.049$, double sided t-test, $t(1431)=-2.2$, $p=0.03$) (Fig.

237 S4c). Collectively, these results demonstrate that the conditioning task is represented in both
238 environments A and B, and that the percentage of cells representing the conditioning task was
239 not different between the two environments.

240 We then examined the overlap between cells that contained spatial information and those
241 with CSUS information, identifying a significant positive correlation between spatial MI and
242 CSUS-MI2 (linear regression, $r^2 = 0.04$, $p=2.1*10^{-104}$) and spatial MI and CSUS-MI5 (linear
243 regression, $r^2 = 0.09$, $p=1.7*10^{-237}$; note that the statistics have been computed for unbinned data
244 but the graph presents binned data for visualization purposes due to the large number of points)
245 (Fig. 4c). Further analysis revealed that cells with significant spatial modulation had a
246 significantly higher likelihood of being significantly modulated by CSUS compared to cells
247 without spatial modulation: 1.35 times higher chance of having significant spatial MI if the cell
248 has a significant CSUS-MI2 (Fisher's exact test, $p=0.001$) and 1.27 times higher chance if the
249 cell has a significant CSUS-MI5 (Fisher's exact test, $p=0.002$). We then inquired whether the
250 calcium events that occurred during conditioning periods were confined to the 'firing' fields of
251 place cells. We thus calculated the average location of calcium events during conditioning
252 periods versus the average location during periods of movement that were not conditioning
253 periods. We analyzed this data using the Mantel test, which statistically evaluates the correlation
254 between two distance matrices to determine if the spatial patterns they represent are significantly
255 related. Across all sessions, we found a Mantel statistic of 534.58; we compared this statistic to
256 the result of 10,000 shuffles to determine the statistic was not significant ($p>0.05$); i.e. the spatial
257 firing patterns during conditioning periods are not generally similar to those that occur during
258 non-conditioning periods (Fig. 4d). In other words, the spatial distribution of firing during

259 conditioning differs fundamentally from that during non-conditioning periods, a result which
260 would not be expected if conditioning related responses were restricted to the cells' place fields

261 We next assessed the consistency of task representation across environments. When we
262 compared cells that appeared in both sessions A(n) and B(1), there was no difference in cell
263 responses to either CS or US (double sided t-tests for CS: $t(1174) = 0.68$ $p > 0.05$ and ks test
264 $p > 0.05$, for US: $t(1174) = 1.20$ $p > 0.05$, and ks-test $p > 0.05$) (Fig. 4e).

265

266 ***Conditioning task representations are consistent across environments***

267 We then trained a CEBRA model using calcium imaging data and time-stamped CS/US
268 periods from environment A, using only cells that were recorded in both environment A and B.
269 We then used this trained model to decode if the animal was in a CS or US period during an
270 additional session in environment A, as well as in environment B. All models successfully
271 decoded CS and US periods the additional session in environment A, as compared to shuffled
272 data (all double sided t-tests, for each rat: rat1: $t(998):6.7$ $p = 2.5 * 10^{-11}$, rat2: $t(998):16.1$
273 $p = 7.4 * 10^{-52}$, rat3: $t(998)=83.5$ $p=0$, rat4: $t(998):80.1$ $p=0$, rat5: $t(998):61.0$ $p=0$) (Fig. 5a,c). All
274 five models significantly outperformed chance level in environment B as determined by shuffled
275 data (all double sided t-tests, for each rat: rat1: $t(998):10.4$ $p = 2.6 * 10^{-24}$, rat2: $t(998):2.7$
276 $p = 7.6 * 10^{-3}$, rat3: $t(998)=75.3$ $p=0$, rat4: $t(998):63.7$ $p=0$, rat5: $t(998):106.3$ $p=0$) (Fig. 5b-c).

277

278 We then trained an additional model on data from environment A during session A(n) to
279 ascertain whether it could decode the temporal order within the conditioning period (CSUS5),
280 both in an alternate session in environment A (session A(n-1)) and in environment B (session

281 B(1)). After being trained on session A(n), all models were able to decode environment A(n-1)
282 well better than chance levels (all double sided t-tests for accuracy, for each rat: rat1: t(998):41.5
283 $p=3.3*10^{-220}$, rat2: t(998):28.7 $p=7.8*10^{-133}$, rat3: t(998)=122.6 $p=0$, rat4: t(998):118.5 $p=0$, rat5:
284 t(998):62.6 $p=0$) (Fig. 5d,f,g). Remarkably, our results for decoding environment B(1) showed
285 that temporal aspects of CS/US temporal order were decodable across environments, suggesting
286 that a refined level of task encoding is stable across both environments (all double sided t-tests
287 for accuracy, for each rat: rat1: t(998):55.1 $p=4.9*10^{-305}$, rat2: t(998):9.3 $p=1.1*10^{-19}$, rat3:
288 t(998)=71.4 $p=0$, rat4: t(998):62.6 $p=0$, rat5: t(998):106.2 $p=0$; results were also significant
289 compared to those for shuffled data for precision, recall, F1 score, and area under the receiver
290 operating characteristic curve, data not shown, see Methods) (Fig. 5e-g).

291
292 Remarkably, for both CSUS2 and CSUS5, the model trained on session A(n) was no less
293 accurate decoding session B(1) than it was decoding session A(n-1) (double sided t-tests, for
294 CSUS2 t(8)=-0.13, $p>0.05$, for CSUS5, t(8)=0.32, $p>0.05$) (Fig. 5h).

295
296 We then used CEBRA to analyze the embedding geometries of cell representations during
297 CS/US periods in both environments. First, we examined the embedding geometries for the
298 conditioning task divided into CS and US periods (CSUS2), for 2, 3, 5, 7, and 10 latents. We
299 compared sessions A(n-1), A(n), B(1), and B(2) to each other, as well as shuffled versions of
300 each session.

301
302 For all 5 rats, the geometries displayed a high and significant degree of similarity as
303 compared to the shuffled control. This significance was maintained when examining up to 10

304 latents, the largest number of latents we utilized (averaging results from all animals, all double
305 sided t-tests, for 2 latents all comparisons were $p < 1 * 10^{-5}$, for 3 latents $p < 1 * 10^{-4}$, for 5 latents
306 $p < 1 * 10^{-5}$, for 7 latents $p < 1 * 10^{-5}$, and for 10 latents $p < 1 * 10^{-4}$) (Fig. 6a-c). This high degree of
307 similarity was maintained when the CS/US periods were divided into 5 segments (CSUS5, (all
308 double sided t-tests, for 2 latents all comparisons were $p < 1 * 10^{-12}$, for 3 latents $p < 1 * 10^{-7}$, for 5
309 latents $p < 1 * 10^{-6}$, for 7 latents $p < 1 * 10^{-5}$, and for 10 latents $p < 1 * 10^{-5}$) (Fig. 6d-f).

310

311 These highly significant similarity signifies that the neural representations of the task
312 were consistent between environments A and B.

313

314 ***Conditioning task representations are consistent across animals***

315 Considering the similarity between representations of the task in environments A and B, we
316 wondered if there was a universal, inter-animal, representation of the conditioning task. To
317 answer this question, we investigated if there were coding similarities of the conditioning task
318 across subjects. For each animal, we developed a unique model based on calcium signal patterns
319 and the structure of the conditioning task. We then calculated a similarity score among all
320 animal-specific models. We observed a markedly significant consistency across these trained
321 models compared to those trained on shuffled data. Notably, this consistency was apparent in
322 models trained to differentiate between CS and US periods, as well as in more granular models
323 that recognized five discrete time segments during CS presentation, the trace interval, and US
324 delivery (akin to the models in Figures 6d-g). When the conditioning period is divided into 2
325 periods (CSUS2), the similarity across animal models is not significantly different than the

326 similarity between models in one animal for all tested number of latents (2 latents: $ttest(188) = -$
327 0.45 $p > 0.05$, 3 latents: $ttest(188) = -1.57$ $p > 0.05$, 5 latents: $ttest(188) = -0.40$ $p > 0.05$, 7 latents:
328 $ttest(188) = -0.22$, $p > 0.05$, 10 latents: $ttest(188) = 0.40$, $p > 0.05$) (Fig. 7a-b). This relationship
329 also holds when the conditioning period is divided into 5 periods (CSUS5): the similarity across
330 animal models is not significantly different than the similarity between models in one animal (2
331 latents: $ttest(188) = -0.79$ $p > 0.05$, 3 latents: $ttest(188) = 0.25$ $p > 0.05$, 5 latents: $ttest(188) = -0.42$
332 $p > 0.05$, 7 latents: $ttest(188) = 0.70$, $p > 0.05$, 10 latents: $ttest(188) = 0.30$, $p > 0.05$) (Fig. 7c-d).

333

334 **Discussion**

335 Our study provides significant insights into hippocampal function, as it demonstrates that
336 the hippocampus not only responds to environmental change with changes in neural coding but
337 also maintains consistent task-related information across varying contexts. These mechanisms
338 underpin cognitive flexibility and the ability to apply learned behaviors in new situations. Below
339 we will discuss this interplay between variability and consistency of representations through
340 several theoretical lenses, including predictive coding and cognitive mapping theories, while
341 exploring the stability of these processes within and across subjects.

342

343 **Task abstraction across environments**

344 A critical aspect of our study highlights that the hippocampus retains stable task
345 representations, such as those required for eyeblink conditioning, despite variations in
346 environmental contexts. This ability to generalize learned tasks across different settings supports
347 models that posit a cognitive map that extends beyond simple spatial navigation, such as the
348 Tolman-Eichenbaum Machine's (TEM)⁵³. According to this model, “spatial” maps integrate
349 task-related information and enable the hippocampus to utilize learned behaviors in novel
350 environments that share cognitive demands but differ in sensory or environmental specifics. This
351 flexible functionality exemplifies the hippocampus' role in abstracting and applying learned
352 knowledge, a hallmark of high-dimensional cognitive mapping. This integrated framework
353 facilitates the adaptation of learned behaviors across diverse contexts, an essential capability for
354 navigating both physical and abstract environments.

355 Our findings further reveal that the hippocampus abstracts task-related information from
356 the surrounding sensory environment and suggests that the hippocampus connects experiences

357 across different contexts by recognizing underlying similarities; these features help generalize
358 learning and adjust behavior. Our results thus support the TEM's perspective that the
359 hippocampus can encode higher-order, abstract information crucial for task execution. The
360 ability to detach task representation from immediate sensory inputs allows for a generalized
361 version of learned information⁵⁴⁻⁵⁶, enhancing the hippocampus's utility in supporting the
362 organism's application of learned skills and behaviors in new albeit similar situations^{55,56}. This
363 capacity for abstraction is indicative of a sophisticated neural coding mechanism and of an
364 adaptable and extensive cognitive mapping system, as it provides a buffer against potential
365 interference that could arise from the myriad of sensory stimuli an organism encounters. By
366 maintaining a conceptual, generalized version of learned information, the hippocampus supports
367 the organism's ability to apply learned skills and behaviors in new situations that share
368 underlying similarities with previous experiences but differ in sensory or contextual details.

369

370 **Pattern Separation vs. Completion**

371 Evidence from various areas of neuroscience has led to the development of a theory of HPC
372 function holding that the HPC treats states that involve equivalent actions or relationships such
373 as similar tasks as equivalent, resulting in learning that is easily transferred between
374 environments^{53-55,57,58}. This theory contrasts with the theory that the HPC acts primarily to
375 perform competitive "pattern separation"⁵⁹⁻⁶³. The prevailing theory as well as the cellular and
376 systems level bases for contextual memory remain to be elucidated. In our study, the distinct
377 coding of different environments by hippocampal place cells provides evidence for pattern
378 separation: the hippocampus differentiates between distinct contexts. This separation reduces
379 interference between memories, allowing for more accurate recall based on specific

380 environmental cues. On the other hand, consistent decoding of the eyeblink task across different
381 environments suggests pattern completion. This process allows the hippocampus to reconstruct a
382 complete memory or learned response from partial or generalized cues, enabling the execution of
383 the learned task even when contextual details change.

384 Our results complement previous work that identifies the HPC as both a pattern
385 completer and a pattern separator. Studies have demonstrated that place cells can differentially
386 represent the same environment when task demands change^{61,64,65}, yet show similar firing
387 patterns when locations have similar task demands⁶⁶. In more recent work⁶⁷, rats were exposed to
388 two distinct environments while performing variations of the same task: approaching object A in
389 the first environment and object B in the second; the study revealed anticorrelated hippocampal
390 firing patterns for events in the two contexts. This suggests that the hippocampus encodes
391 context-specific associations between items and locations, rather than just specific behavior. This
392 study underscored the role of the hippocampus in robust pattern separation when environments
393 differ but require similar behaviors, showing that even minor task variations can lead to
394 significant neuronal pattern separation⁶⁷. In contrast, our study used a task that remained
395 identical across both environments and found consistent hippocampal population-level task
396 representations in both contexts. This consistency likely reflects that the task could be
397 generalized between environments, without necessitating the hippocampus to differentiate
398 between task demands. Therefore, the hippocampus seems to balance pattern separation and
399 completion based on how similar or distinct task demands are across different contexts.

400

401 **Non-spatial hippocampal representations**

402 There is ongoing debate about whether hippocampal pyramidal cells encode both spatial
403 and non-spatial aspects of a context^{39,68,69}. Our findings show that responses to the conditioning
404 task were independent of place field location, with a fraction of the recorded individual cells
405 found able to represent both spatial location and the conditioning task (Fig. 4). This contrasts
406 with studies where conditioning responses were more closely tied to specific spatial
407 locations^{70,71}. The difference likely stems from task design: in previous studies, spatially
408 contingent rewards or freezing behavior after a shock made location highly salient, by
409 associating the place where the shock occurred with the aversive event. In our experiment,
410 spatial position was irrelevant; this allowed pyramidal cells to encode task-relevant features
411 independent of location. This finding aligns with previous work showing that hippocampal cells
412 often respond to non-spatial aspects like sensory cues or task demands, particularly in non-spatial
413 tasks^{19,72-74}.

414 The discovery that population level patterns in the hippocampus are organized into
415 manifolds provides an elegant solution to the problem of single cells representing both spatial
416 coordinates and task features. Previous hippocampal work has described distinct encoding for
417 spatial location along the center stem of a T maze vs accumulation of evidence for a left-right
418 turning decision at the end of this branch through two distinct, orthogonal directions in a two-
419 dimensional neural manifold⁷⁵. Other brain regions, such as the prefrontal cortex and cingulate
420 cortex, appear to use a similar orthogonal coding strategy⁷⁶⁻⁷⁸; this strategy has also emerged in
421 neural network simulations of a context-dependent classification task⁷⁹.

422

423 **Intra-Subject and Inter-Subject Consistency**

424 The stability of neural representations within subjects across different testing sessions
425 indicates that once hippocampal circuits are trained, their functional architecture remains
426 remarkably consistent, even in varying contexts. This intra-subject consistency supports theories
427 suggesting that neural circuits are not just reactive but possess a robust, predefined role in
428 processing and responding to specific stimuli^{80,81}. Furthermore, the observation of similar neural
429 encoding patterns across different animals performing the same task suggests a species specific,
430 possibly evolutionary conserved, neural code^{80,81}. These findings highlight a generalized neural
431 processing strategy that may have been shaped by natural selection to optimize cognitive and
432 behavioral responses across environmental challenges faced by a species. Such a generalized
433 coding strategy may be indicative of evolutionary pressures that have favored neural mechanisms
434 promoting cognitive flexibility and rapid adaptation to environmental challenges⁸²⁻⁸⁴.

435 The results of our study highlight the preservation of hippocampal task encoding across
436 different contexts and species; this presents a surprising parallel to recent findings in motor
437 cortex^{85,86} and insular cortex⁸⁷. Motor functions, especially those fundamental to survival and
438 interaction with the physical environment, are expected to exhibit conserved neural dynamics
439 due to their innate and reflexive nature; motor tasks typically involve stereotyped and predictable
440 patterns of behavior that are essential for immediate responses and interactions with the
441 environment⁸⁸⁻⁹¹. Similarly, the motivational states preserved across animals in the insular cortex
442 are those central to basic biological needs, such as thirst and hunger. These states and tasks are
443 often highly conserved across individuals because they rely on well-established neural circuits
444 that perform specific, crucial functions necessary for survival^{89,91-95}.

445 In contrast, hippocampal tasks involve complex cognitive processes that include memory,
446 learning, and spatial navigation; these require a higher degree of cognitive flexibility^{83,96-98}. and

447 are generally influenced by individual experiences (and, at the species level, specific ecological
448 and evolutionary pressures)⁹⁹⁻¹⁰³. Therefore, the conservation of hippocampal task encoding
449 across different individuals, as observed in our study, challenges these traditional views and
450 suggests a deeper, possibly adaptive significance to these cognitive functions.

451 The surprising conservation of the neural representation of tasks within the hippocampus
452 suggests that certain aspects of cognitive mapping and memory processing might be as
453 evolutionarily essential as motor functions. This conservation might reflect universal cognitive
454 strategies that are critical for survival across a range of environmental contexts, providing
455 individuals within a species with the ability to adapt behavior based on past experiences and
456 anticipated future conditions. Such a mechanism would not only enhance an organism's ability to
457 navigate complex environments but also facilitate learning and decision-making across
458 generational timescales.

459

460 **Conclusion**

461

462 The consistent decoding of eyeblink conditioning tasks across different environmental
463 contexts indicates that the hippocampus can maintain a stable representation of task-specific
464 information irrespective of the external sensory environment. This suggests an advanced
465 capability for abstract cognitive mapping, where the hippocampus constructs and utilizes
466 cognitive maps not only for physical locations but also for abstract tasks and concepts, allowing
467 for effective application in varying contexts. These findings expand our understanding of how
468 memories are formed, stored, and retrieved. They suggest that memories are not just static

469 recollections of past events but dynamic and adaptable representations that can be applied to new

470 situations.

471

472

473

474 **Citations**

- 475 1 Bouton, M. E. A learning theory perspective on lapse, relapse, and the maintenance of
476 behavior change. *Health psychology* **19**, 57 (2000).
- 477 2 Herszage, J. & Censor, N. Modulation of learning and memory: a shared framework for
478 interference and generalization. *Neuroscience* **392**, 270-280 (2018).
- 479 3 Linda, Q. Y., Wilson, R. C. & Nassar, M. R. Adaptive learning is structure learning in time.
480 *Neuroscience & Biobehavioral Reviews* **128**, 270-281 (2021).
- 481 4 Censor, N. Generalization of perceptual and motor learning: a causal link with memory
482 encoding and consolidation? *Neuroscience* **250**, 201-207 (2013).
- 483 5 Brown, S. & Bebkco, J. Generalization, overselectivity, and discrimination in the autism
484 phenotype: A review. *Research in Autism Spectrum Disorders* **6**, 733-740 (2012).
- 485 6 Church, B. A. *et al.* Learning, plasticity, and atypical generalization in children with
486 autism. *Psychonomic Bulletin & Review* **22**, 1342-1348 (2015).
- 487 7 Weiler, J. A., Bellebaum, C., Brüne, M., Juckel, G. & Daum, I. Impairment of probabilistic
488 reward-based learning in schizophrenia. *Neuropsychology* **23**, 571 (2009).
- 489 8 Shohamy, D. *et al.* Learning and generalization in schizophrenia: effects of disease and
490 antipsychotic drug treatment. *Biological psychiatry* **67**, 926-932 (2010).
- 491 9 Anastasides, N. *et al.* Increased generalization of learned associations is related to re-
492 experiencing symptoms in veterans with symptoms of post-traumatic stress. *Stress* **18**,
493 484-489 (2015).
- 494 10 Lis, S. *et al.* Generalization of fear in post-traumatic stress disorder. *Psychophysiology*
495 **57**, e13422 (2020).
- 496 11 Calandreau, L., Desgranges, B., Jaffard, R. & Desmedt, A. Switching from contextual to
497 tone fear conditioning and vice versa: the key role of the glutamatergic hippocampal-
498 lateral septal neurotransmission. *Learn Mem* **17**, 440-443 (2010).
499 <https://doi.org/10.1101/lm.1859810>
- 500 12 Desmedt, A., Garcia, R. & Jaffard, R. Vasopressin in the lateral septum promotes
501 elemental conditioning to the detriment of contextual fear conditioning in mice. *Eur J*
502 *Neurosci* **11**, 3913-3921 (1999).
- 503 13 Vouimba, R. M., Garcia, R. & Jaffard, R. Opposite effects of lateral septal LTP and lateral
504 septal lesions on contextual fear conditioning in mice. *Behav Neurosci* **112**, 875-884
505 (1998).
- 506 14 Anagnostaras, S. G., Gale, G. D. & Fanselow, M. S. Hippocampus and contextual fear
507 conditioning: recent controversies and advances. *Hippocampus* **11**, 8-17 (2001).
508 [https://doi.org/10.1002/1098-1063\(2001\)11:1<8::AID-HIPO1015>3.0.CO;2-7](https://doi.org/10.1002/1098-1063(2001)11:1<8::AID-HIPO1015>3.0.CO;2-7)
- 509 15 Honey, R. C. & Good, M. Selective hippocampal lesions abolish the contextual specificity
510 of latent inhibition and conditioning. *Behav Neurosci* **107**, 23-33 (1993).
511 <https://doi.org/10.1037//0735-7044.107.1.23>
- 512 16 Plitt, M. H. & Giocomo, L. M. Experience-dependent contextual codes in the
513 hippocampus. *Nat Neurosci* **24**, 705-714 (2021). [https://doi.org/10.1038/s41593-021-](https://doi.org/10.1038/s41593-021-00816-6)
514 [00816-6](https://doi.org/10.1038/s41593-021-00816-6)

- 515 17 Devito, L. M., Kanter, B. R. & Eichenbaum, H. The hippocampus contributes to memory
516 expression during transitive inference in mice. *Hippocampus* **20**, 208-217 (2010).
517 <https://doi.org/10.1002/hipo.20610>
- 518 18 Schimanski, L. A., Lipa, P. & Barnes, C. A. Tracking the course of hippocampal
519 representations during learning: when is the map required? *J Neurosci* **33**, 3094-3106
520 (2013). <https://doi.org/10.1523/JNEUROSCI.1348-12.2013>
- 521 19 Gauthier, J. L. & Tank, D. W. A Dedicated Population for Reward Coding in the
522 Hippocampus. *Neuron* **99**, 179-193 e177 (2018).
523 <https://doi.org/10.1016/j.neuron.2018.06.008>
- 524 20 Mamad, O. *et al.* Place field assembly distribution encodes preferred locations. *PLoS Biol*
525 **15**, e2002365 (2017). <https://doi.org/10.1371/journal.pbio.2002365>
- 526 21 Hok, V. *et al.* Goal-related activity in hippocampal place cells. *J Neurosci* **27**, 472-482
527 (2007). <https://doi.org/10.1523/JNEUROSCI.2864-06.2007> [pii]
- 528 22 Knierim, J. J. Dynamic interactions between local surface cues, distal landmarks, and
529 intrinsic circuitry in hippocampal place cells. *J Neurosci* **22**, 6254-6264 (2002).
530 <https://doi.org/10.1523/JNEUROSCI.2864-06.2007>
- 531 23 Allen, K., Rawlins, J. N., Bannerman, D. M. & Csicsvari, J. Hippocampal place cells can
532 encode multiple trial-dependent features through rate remapping. *J Neurosci* **32**, 14752-
533 14766 (2012). <https://doi.org/10.1523/JNEUROSCI.6175-11.2012>
- 534 24 Jeffery, K. J., Gilbert, A., Burton, S. & Strudwick, A. Preserved performance in a
535 hippocampal-dependent spatial task despite complete place cell remapping.
536 *Hippocampus* **13**, 175-189 (2003). <https://doi.org/10.1002/hipo.10047>
- 537 25 Colgin, L. L., Moser, E.I., May-Britt Moser. Understanding memory through hippocampal
538 remapping. *Cell* (2008).
- 539 26 Christian, K. M. & Thompson, R. F. Neural substrates of eyeblink conditioning:
540 acquisition and retention. *Learn Mem* **10**, 427-455 (2003).
541 <https://doi.org/10.1101/lm.59603>
- 542 27 McEchron, M. D., Tseng, W. & Disterhoft, J. F. Single neurons in CA1 hippocampus
543 encode trace interval duration during trace heart rate (fear) conditioning in rabbit. *J*
544 *Neurosci* **23**, 1535-1547 (2003).
- 545 28 Wirtshafter, H. S. & Wilson, M. A. Locomotor and Hippocampal Processing Converge in
546 the Lateral Septum. *Current biology : CB* **29**, 3177-3192 (2019).
547 <https://doi.org/10.1016/j.cub.2019.07.089>
- 548 29 Berger, T. W., Rinaldi, P. C., Weisz, D. J. & Thompson, R. F. Single-unit analysis of
549 different hippocampal cell types during classical conditioning of rabbit nictitating
550 membrane response. *J Neurophysiol* **50**, 1197-1219 (1983).
551 <https://doi.org/10.1152/jn.1983.50.5.1197>
- 552 30 Wirtshafter, H. S. & Wilson, M. A. Differences in reward biased spatial representations in
553 the lateral septum and hippocampus. *eLife* **9** (2020).
554 <https://doi.org/10.7554/eLife.55252>
- 555 31 Wirtshafter, H. S. & Disterhoft, J. F. Place cells are nonrandomly clustered by field
556 location in CA1 hippocampus. *Hippocampus* **33**, 65-84 (2023).
557 <https://doi.org/10.1002/hipo.23489>

- 558 32 Aharoni, D. & Hoogland, T. M. Circuit Investigations With Open-Source Miniaturized
559 Microscopes: Past, Present and Future. *Frontiers in cellular neuroscience* **13**, 141 (2019).
560 <https://doi.org/10.3389/fncel.2019.00141>
- 561 33 Aharoni, D., Khakh, B. S., Silva, A. J. & Golshani, P. All the light that we can see: a new
562 era in miniaturized microscopy. *Nat Methods* **16**, 11-13 (2019).
563 <https://doi.org/10.1038/s41592-018-0266-x>
- 564 34 Silva, A. J. Miniaturized two-photon microscope: seeing clearer and deeper into the
565 brain. *Light: Science & Applications* **6**, e17104-e17104 (2017).
- 566 35 Wirtshafter, H. S. & Disterhoft, J. F. In Vivo Multi-Day Calcium Imaging of CA1
567 Hippocampus in Freely Moving Rats Reveals a High Preponderance of Place Cells with
568 Consistent Place Fields. *J Neurosci* (2022). [https://doi.org/doi:10.1523/JNEUROSCI.1750-](https://doi.org/doi:10.1523/JNEUROSCI.1750-21.2022)
569 [21.2022](https://doi.org/doi:10.1523/JNEUROSCI.1750-21.2022)
- 570 36 Cunningham, J. P. & Byron, M. Y. Dimensionality reduction for large-scale neural
571 recordings. *Nature neuroscience* **17**, 1500-1509 (2014).
- 572 37 Bassett, D. S. & Sporns, O. Network neuroscience. *Nature neuroscience* **20**, 353-364
573 (2017).
- 574 38 Ekstrom, A. D. & Ranganath, C. Space, time, and episodic memory: The hippocampus is
575 all over the cognitive map. *Hippocampus* **28**, 680-687 (2018).
- 576 39 Eichenbaum, H., Dudchenko, P., Wood, E., Shapiro, M. & Tanila, H. The hippocampus,
577 memory, and place cells: is it spatial memory or a memory space? *Neuron* **23**, 209-226
578 (1999). [https://doi.org/S0896-6273\(00\)80773-4](https://doi.org/S0896-6273(00)80773-4) [pii]
- 579 40 Fenton, A. A. Remapping revisited: how the hippocampus represents different spaces.
580 *Nat Rev Neurosci* **25**, 428-448 (2024). <https://doi.org/10.1038/s41583-024-00817-x>
- 581 41 Sanders, H., Wilson, M. A. & Gershman, S. J. Hippocampal remapping as hidden state
582 inference. *eLife* **9** (2020). <https://doi.org/10.7554/eLife.51140>
- 583 42 Bouton, M. E., Nelson, J. B. & Rosas, J. M. Stimulus generalization, context change, and
584 forgetting. *Psychological bulletin* **125**, 171-186 (1999). [https://doi.org/10.1037/0033-](https://doi.org/10.1037/0033-2909.125.2.171)
585 [2909.125.2.171](https://doi.org/10.1037/0033-2909.125.2.171)
- 586 43 Lovibond, P. F., Preston, G. & Mackintosh, N. Context specificity of conditioning,
587 extinction, and latent inhibition. *Journal of Experimental Psychology: Animal Behavior*
588 *Processes* **10**, 360 (1984).
- 589 44 Moyer, J. R., Jr., Deyo, R. A. & Disterhoft, J. F. Hippocampectomy disrupts trace eye-blink
590 conditioning in rabbits. *Behav Neurosci* **104**, 243-252 (1990).
- 591 45 McEchron, M. D. & Disterhoft, J. F. Hippocampal encoding of non-spatial trace
592 conditioning. *Hippocampus* **9**, 385-396 (1999). [https://doi.org/10.1002/\(SICI\)1098-](https://doi.org/10.1002/(SICI)1098-1063(1999)9:4<385::AID-HIPO5>3.0.CO;2-K)
593 [1063\(1999\)9:4<385::AID-HIPO5>3.0.CO;2-K](https://doi.org/10.1002/(SICI)1098-1063(1999)9:4<385::AID-HIPO5>3.0.CO;2-K)
- 594 46 Woodruff-Pak, D. S. & Disterhoft, J. F. Where is the trace in trace conditioning? *Trends*
595 *Neurosci* **31**, 105-112 (2008). <https://doi.org/10.1016/j.tins.2007.11.006>
- 596 47 Weiss, C. & Disterhoft, J. F. The impact of hippocampal lesions on trace-eyeblink
597 conditioning and forebrain-cerebellar interactions. *Behav Neurosci* **129**, 512-522 (2015).
598 <https://doi.org/10.1037/bne0000061>
- 599 48 Neymotin, S. A., Talbot, Z. N., Jung, J. Q., Fenton, A. A. & Lytton, W. W. Tracking
600 recurrence of correlation structure in neuronal recordings. *J Neurosci Methods* **275**, 1-9
601 (2017). <https://doi.org/10.1016/j.jneumeth.2016.10.009>

- 602 49 Brun, V. H. *et al.* Progressive increase in grid scale from dorsal to ventral medial
603 entorhinal cortex. *Hippocampus* **18**, 1200-1212 (2008).
604 <https://doi.org/10.1002/hipo.20504>
- 605 50 Schneider, S., Lee, J. H. & Mathis, M. W. Learnable latent embeddings for joint
606 behavioural and neural analysis. *Nature* **617**, 360-368 (2023).
607 <https://doi.org/10.1038/s41586-023-06031-6>
- 608 51 Pearson, K. LIII. On lines and planes of closest fit to systems of points in space. *The*
609 *London, Edinburgh, and Dublin philosophical magazine and journal of science* **2**, 559-572
610 (1901).
- 611 52 Tenenbaum, J. B., Silva, V. d. & Langford, J. C. A global geometric framework for
612 nonlinear dimensionality reduction. *science* **290**, 2319-2323 (2000).
- 613 53 Whittington, J. C. R. *et al.* The Tolman-Eichenbaum Machine: Unifying Space and
614 Relational Memory through Generalization in the Hippocampal Formation. *Cell* **183**,
615 1249-1263 e1223 (2020). <https://doi.org/10.1016/j.cell.2020.10.024>
- 616 54 Wirtshafter, H. S. & Wilson, M. A. Artificial intelligence insights into hippocampal
617 processing. *Front Comput Neurosci* **16**, 1044659 (2022).
618 <https://doi.org/10.3389/fncom.2022.1044659>
- 619 55 Lehnert, L., Littman, M. L. & Frank, M. J. Reward-predictive representations generalize
620 across tasks in reinforcement learning. *PLoS Comput Biol* **16**, e1008317 (2020).
621 <https://doi.org/10.1371/journal.pcbi.1008317>
- 622 56 Collins, A. G. E. & Frank, M. J. Neural signature of hierarchically structured expectations
623 predicts clustering and transfer of rule sets in reinforcement learning. *Cognition* **152**,
624 160-169 (2016).
- 625 57 Stachenfeld, K. L., Botvinick, M. M. & Gershman, S. J. The hippocampus as a predictive
626 map. *Nat Neurosci* **20**, 1643-1653 (2017). <https://doi.org/10.1038/nn.4650>
- 627 58 Eichenbaum, H. Hippocampus: cognitive processes and neural representations that
628 underlie declarative memory. *Neuron* **44**, 109-120 (2004).
- 629 59 Wills, T. J., Lever, C., Cacucci, F., Burgess, N. & O'Keefe, J. Attractor dynamics in the
630 hippocampal representation of the local environment. *Science* **308**, 873-876 (2005).
631 <https://doi.org/10.1126/science.1108905>
- 632 60 Colgin, L. L. *et al.* Attractor-map versus autoassociation based attractor dynamics in the
633 hippocampal network. *J Neurophysiol* **104**, 35-50 (2010).
634 <https://doi.org/10.1152/jn.00202.2010>
- 635 61 Smith, D. M. & Mizumori, S. J. Learning-related development of context-specific
636 neuronal responses to places and events: the hippocampal role in context processing. *J*
637 *Neurosci* **26**, 3154-3163 (2006). <https://doi.org/10.1523/JNEUROSCI.3234-05.2006>
- 638 62 Colgin, L. L. *et al.* Attractor-map versus autoassociation based attractor dynamics in the
639 hippocampal network. *Journal of neurophysiology* **104**, 35-50 (2010).
- 640 63 Lee, I., Yoganarasimha, D., Rao, G. & Knierim, J. J. Comparison of population coherence
641 of place cells in hippocampal subfields CA1 and CA3. *Nature* **430**, 456-459 (2004).
- 642 64 Bahar, A. S., Shirvalkar, P. R. & Shapiro, M. L. Memory-guided learning: CA1 and CA3
643 neuronal ensembles differentially encode the commonalities and differences between
644 situations. *J Neurosci* **31**, 12270-12281 (2011).
645 <https://doi.org/10.1523/JNEUROSCI.1671-11.2011>

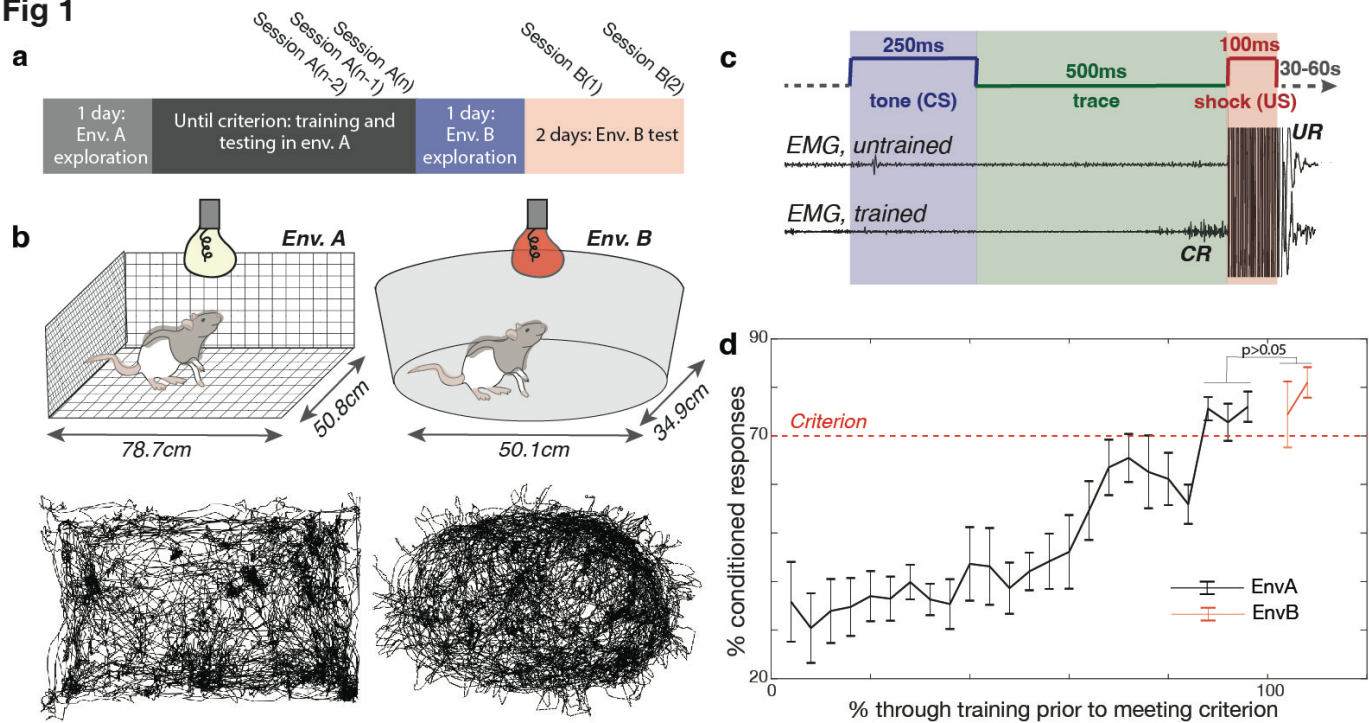
- 646 65 Markus, E. J. *et al.* Interactions between location and task affect the spatial and
647 directional firing of hippocampal neurons. *J Neurosci* **15**, 7079-7094 (1995).
- 648 66 Singer, A. C., Karlsson, M. P., Nathe, A. R., Carr, M. F. & Frank, L. M. Experience-
649 dependent development of coordinated hippocampal spatial activity representing the
650 similarity of related locations. *J Neurosci* **30**, 11586-11604 (2010).
651 <https://doi.org/10.1523/JNEUROSCI.0926-10.2010>
- 652 67 McKenzie, S. *et al.* Hippocampal representation of related and opposing memories
653 develop within distinct, hierarchically organized neural schemas. *Neuron* **83**, 202-215
654 (2014). <https://doi.org/10.1016/j.neuron.2014.05.019>
- 655 68 O'Keefe, J. & Krupic, J. Do hippocampal pyramidal cells respond to nonspatial stimuli?
656 *Physiol Rev* **101**, 1427-1456 (2021). <https://doi.org/10.1152/physrev.00014.2020>
- 657 69 Knierim, J. J. From the GPS to HM: Place cells, grid cells, and memory. *Hippocampus* **25**,
658 719-725 (2015). <https://doi.org/10.1002/hipo.22453>
- 659 70 Moita, M. A., Rosis, S., Zhou, Y., LeDoux, J. E. & Blair, H. T. Hippocampal place cells
660 acquire location-specific responses to the conditioned stimulus during auditory fear
661 conditioning. *Neuron* **37**, 485-497 (2003). [https://doi.org/10.1016/s0896-
662 6273\(03\)00033-3](https://doi.org/10.1016/s0896-6273(03)00033-3)
- 663 71 Shan, K. Q., Lubenov, E. V., Papadopoulou, M. & Siapas, A. G. Spatial tuning and brain
664 state account for dorsal hippocampal CA1 activity in a non-spatial learning task. *eLife* **5**
665 (2016). <https://doi.org/10.7554/eLife.14321>
- 666 72 Wood, E. R., Dudchenko, P. A. & Eichenbaum, H. The global record of memory in
667 hippocampal neuronal activity. *Nature* **397**, 613-616 (1999).
668 <https://doi.org/10.1038/17605>
- 669 73 Kennedy, P. J. & Shapiro, M. L. Motivational states activate distinct hippocampal
670 representations to guide goal-directed behaviors. *Proc Natl Acad Sci U S A* **106**, 10805-
671 10810 (2009). <https://doi.org/10.1073/pnas.0903259106>
- 672 74 Holscher, C., Jacob, W. & Mallot, H. A. Reward modulates neuronal activity in the
673 hippocampus of the rat. *Behav Brain Res* **142**, 181-191 (2003).
- 674 75 Nieh, E. H. *et al.* Geometry of abstract learned knowledge in the hippocampus. *Nature*
675 **595**, 80-84 (2021).
- 676 76 Johnston, W. J., Fine, J. M., Yoo, S. B. M., Ebitz, R. B. & Hayden, B. Y. Semi-orthogonal
677 subspaces for value mediate a binding and generalization trade-off. *Nature*
678 *Neuroscience*, 1-13 (2024).
- 679 77 Machens, C. K., Romo, R. & Brody, C. D. Functional, but not anatomical, separation of
680 “what” and “when” in prefrontal cortex. *Journal of Neuroscience* **30**, 350-360 (2010).
- 681 78 Mante, V., Sussillo, D., Shenoy, K. V. & Newsome, W. T. Context-dependent computation
682 by recurrent dynamics in prefrontal cortex. *nature* **503**, 78-84 (2013).
- 683 79 Flesch, T., Juechems, K., Dumbalska, T., Saxe, A. & Summerfield, C. Orthogonal
684 representations for robust context-dependent task performance in brains and neural
685 networks. *Neuron* **110**, 1258-1270. e1211 (2022).
- 686 80 Mizumori, S. J., Canfield, J. G. & Yeshenko, O. Parallel and interrelated neural systems
687 underlying adaptive navigation. *Integrative and Comparative Biology* **45**, 547-554
688 (2005).

- 689 81 Mizumori, S. J., Cooper, B. G., Leutgeb, S. & Pratt, W. E. A neural systems analysis of
690 adaptive navigation. *Mol Neurobiol* **21**, 57-82 (2000). [https://doi.org/10.1385/MN:21:1-](https://doi.org/10.1385/MN:21:1-2:057)
691 [2:057](https://doi.org/10.1385/MN:21:1-2:057)
- 692 82 Mizumori, S. & Smith, D. Directing Neural Representations of Space. *Animal Spatial*
693 *Cognition: Comparative, Neural, and Computational Approaches* (2006).
- 694 83 Buzsáki, G. & Moser, E. I. Memory, navigation and theta rhythm in the hippocampal-
695 entorhinal system. *Nature neuroscience* **16**, 130-138 (2013).
- 696 84 Bunsey, M. & Eichenbaum, H. Conservation of hippocampal memory function in rats and
697 humans. *Nature* **379**, 255-257 (1996). <https://doi.org/10.1038/379255a0>
- 698 85 Safaie, M. *et al.* Preserved neural dynamics across animals performing similar behaviour.
699 *Nature* **623**, 765-771 (2023). <https://doi.org/10.1038/s41586-023-06714-0>
- 700 86 Gallego, J. A. *et al.* Cortical population activity within a preserved neural manifold
701 underlies multiple motor behaviors. *Nature communications* **9**, 1-13 (2018).
- 702 87 Talpir, I. & Livneh, Y. Stereotyped goal-directed manifold dynamics in the insular cortex.
703 *Cell reports* **43** (2024).
- 704 88 Kogan, E., Lu, J. & Zuo, Y. Cortical circuit dynamics underlying motor skill learning: from
705 rodents to humans. *Frontiers in Molecular Neuroscience* **16**, 1292685 (2023).
- 706 89 Manoli, D. S., Meissner, G. W. & Baker, B. S. Blueprints for behavior: genetic
707 specification of neural circuitry for innate behaviors. *Trends in neurosciences* **29**, 444-
708 451 (2006).
- 709 90 LeDoux, J. & Daw, N. D. Surviving threats: neural circuit and computational implications
710 of a new taxonomy of defensive behaviour. *Nature Reviews Neuroscience* **19**, 269-282
711 (2018).
- 712 91 LeDoux, J. E. As soon as there was life, there was danger: the deep history of survival
713 behaviours and the shallower history of consciousness. *Philosophical Transactions of the*
714 *Royal Society B* **377**, 20210292 (2022).
- 715 92 Harris, K. D. & Shepherd, G. M. The neocortical circuit: themes and variations. *Nature*
716 *neuroscience* **18**, 170-181 (2015).
- 717 93 Shmuelof, L. & Krakauer, J. W. Are we ready for a natural history of motor learning?
718 *Neuron* **72**, 469-476 (2011).
- 719 94 Tierney, A. Evolutionary implications of neural circuit structure and function.
720 *Behavioural processes* **35**, 173-182 (1995).
- 721 95 Martínez-García, F. & Lanuza, E. Evolution of vertebrate survival circuits. *Current Opinion*
722 *in Behavioral Sciences* **24**, 113-123 (2018).
- 723 96 Sweis, B. M., Mau, W., Rabinowitz, S. & Cai, D. J. Dynamic and heterogeneous neural
724 ensembles contribute to a memory engram. *Curr Opin Neurobiol* **67**, 199-206 (2021).
725 <https://doi.org/10.1016/j.conb.2020.11.017>
- 726 97 Davidson, T. J., Kloosterman, F. & Wilson, M. A. Hippocampal replay of extended
727 experience. *Neuron* **63**, 497-507 (2009). <https://doi.org/10.1016/j.neuron.2009.07.027>
728 S0896-6273(09)00582-0 [pii]
- 729 98 Rubin, R. D., Watson, P. D., Duff, M. C. & Cohen, N. J. The role of the hippocampus in
730 flexible cognition and social behavior. *Frontiers in human neuroscience* **8**, 742 (2014).
- 731 99 Poulter, S., Hartley, T. & Lever, C. The neurobiology of mammalian navigation. *Current*
732 *Biology* **28**, R1023-R1042 (2018).

- 733 100 Tucker, M. A., Ord, T. J. & Rogers, T. L. Evolutionary predictors of mammalian home
734 range size: body mass, diet and the environment. *Global Ecology and Biogeography* **23**,
735 1105-1114 (2014).
- 736 101 Schilder, B. M., Petry, H. M. & Hof, P. R. Evolutionary shifts dramatically reorganized the
737 human hippocampal complex. *Journal of Comparative Neurology* **528**, 3143-3170
738 (2020).
- 739 102 Sherry, D. F., Jacobs, L. F. & Gaulin, S. J. Spatial memory and adaptive specialization of
740 the hippocampus. *Trends in neurosciences* **15**, 298-303 (1992).
- 741 103 Pravosudov, V. V. & Roth II, T. C. Cognitive ecology of food hoarding: the evolution of
742 spatial memory and the hippocampus. *Annual Review of Ecology, Evolution, and*
743 *Systematics* **44**, 173-193 (2013).
744

745

Fig 1



747 **Fig 1. Experimental training paradigm and results.**

748 **a.** Animals explored environment A for one session before undergoing eyeblink
 749 conditioning until they reached the learning criterion. Criterion was defined as achieving
 750 70% conditioned responses (CRs) in 50 trials across three consecutive training sessions
 751 (A(n-2), A(n-1), and A(n)) or averaging over 70% CRs across the previous four training
 752 sessions. After meeting the criterion in environment A, animals were allowed one session
 753 of exploration in environment B, followed by two test sessions of trace eyeblink
 754 conditioning (B(1) and B(2)) in environment B.

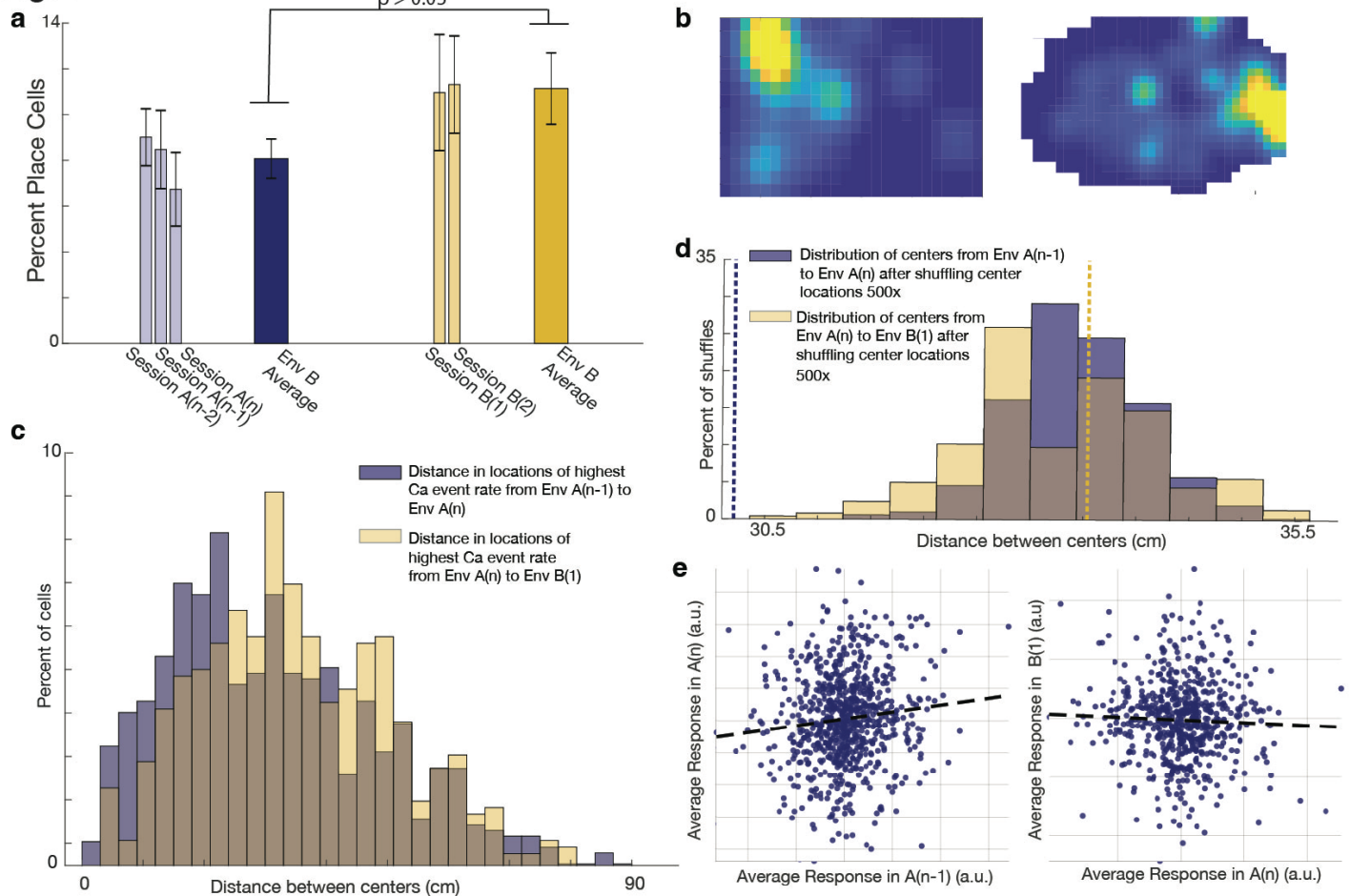
755 **b.** (Top) Schematics of environments A and B. Environment A is a rectangular enclosure
 756 with wire walls, floor, and ceiling, lit with white light, and unscented. Environment B is
 757 oval-shaped with solid white floors and walls, without a ceiling, lit with red light, and
 758 scented with clove oil. Both environments provided distal cues visible from the top and

759 sides. (Bottom) Animal trajectories in environments A and B during a single session,
760 extracted using DeepLabCut.

761 **c.** Trace eyeblink conditioning (tEBC) paradigm. A 250 ms tone (conditioned stimulus, CS)
762 was followed by a 500 ms trace interval, then a 100 ms eyelid shock (unconditioned
763 stimulus, US). Eyelid activity was recorded using an EMG electrode implanted above the
764 eye. Untrained animals only blinked in response to the US (unconditioned response, UR);
765 trained animals began blinking during the trace interval after the CS and before the US
766 (conditioned response, CR).

767 **d.** Performance of animals (n=5) in the tEBC task. Animals learned tEBC while freely
768 moving in environment A and successfully transferred this learning to environment B.
769 The dotted line indicates the performance criterion. No significant difference was found
770 between performance in the criterion sessions in environment A (mean $74.75 \pm 6.49\%$)
771 and the test sessions in environment B (mean $77.70 \pm 11.68\%$; two-tailed t-test, $t(24) = -$
772 0.83 , $p > 0.05$). Error bars represent standard error.

Fig 2

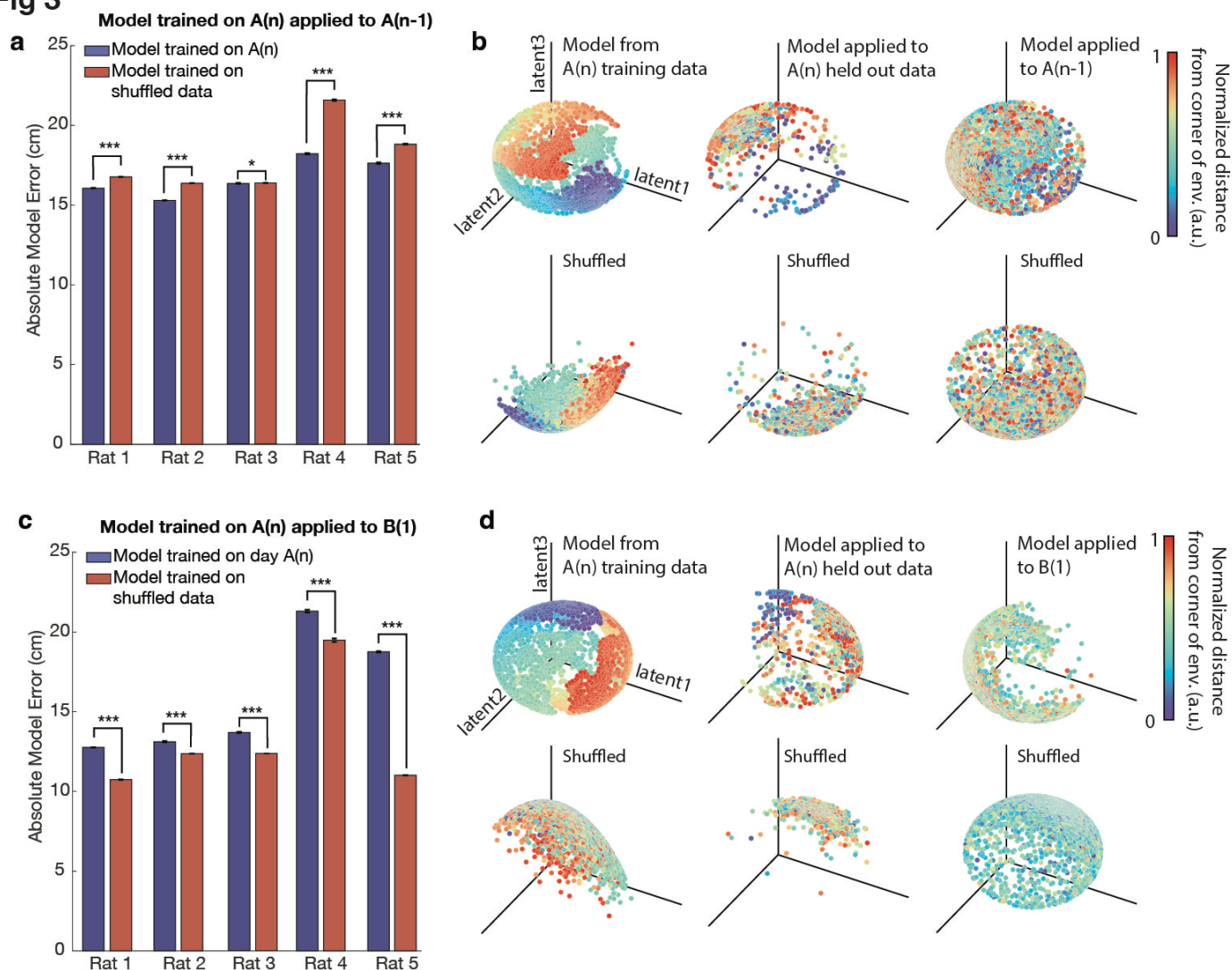


774 **Fig 2. Place cells remap between environment A and environment B.**

775 **a.** Percent of place cells during criterion sessions in environment A and test sessions in
 776 environment B. Light-colored bars represent averages within individual sessions, and
 777 dark-colored bars represent overall averages in environments A and B. Overlaid bars
 778 indicate standard deviation. On average, $9.3\% \pm 4.2\%$ of cells were classified as place
 779 cells. There was no significant difference in the percentage of place cells between
 780 environments A and B (average in environment A: $8.1\% \pm 3.3\%$; average in environment
 781 B: $11.1\% \pm 4.9\%$; two-tailed t-test, $t(23) = -1.9$, $p > 0.05$).

- 782 **b.** Example activity map of a specific single cell in environments A and B. Yellow indicates
783 the highest firing rates. This cell exhibited remapping between environments, showing
784 different place fields relative to external cues in the two contexts.
- 785 **c.** Distribution of distances between place field centers (determined by the highest calcium
786 event rate), comparing sessions A(n) and A(n-1) versus sessions A(n) and B(1). Place
787 field centers shifted significantly more when the animal was moved to environment B
788 compared to shifts between two consecutive sessions in environment A (Wilcoxon rank
789 sum test, $p = 0.002$; two-sided t-test, $t(1430) = -2.5$, $p = 0.01$; two-sample Kolmogorov-
790 Smirnov test, $p = 3.6 \times 10^{-10}$). The brown shaded area represents the overlap between
791 distance histograms.
- 792 **d.** Distribution of the median distance between place field centers after shuffling center
793 locations 500 times. The actual median value for session A(n) to A(n-1) was smaller than
794 all shuffled medians ($p = 0$, dashed blue line), while the median for session A(n) to B(1)
795 was greater than or equal to 56% of shuffled medians ($p = 0.56$, dashed yellow line). The
796 brown shaded area represents the overlap between shuffled distributions.
- 797 **e.** Population vector correlation (PVC) based on calcium events for sessions A(n-1), A(n),
798 and B(1). A significant positive correlation was found between sessions A(n-1) and A(n)
799 for cells present in both sessions ($p = 0.0023$, $r = 0.11$). In contrast, there was no
800 significant correlation between sessions A(n) and B(1) for shared cells ($p > 0.05$, $r = -$
801 0.04). These findings suggest that calcium event patterns are significantly similar
802 between sessions A(n-1) and A(n) but not between session A(n) and B(1). Dashed lines
803 represent lines of best fit. (a.u. = arbitrary units).
- 804

Fig 3



806 **Fig. 3. A model trained in environment A can decode positions within environment A but**
 807 **not in environment B.**

808 **a.** A model trained on calcium trace and position data from session A(n), using cells present
 809 in both A(n) and A(n-1), predicted positions in environment A(n-1) with significantly
 810 greater accuracy than that of a model trained on shuffled position data. The model was
 811 run 500 times, and the accuracy of predictions was assessed. The model trained on actual
 812 data significantly outperformed the shuffled model across rats (double-sided t-tests: Rat
 813 1: $t(998) = -34.3$, $p = 5.0 \times 10^{-171}$; Rat 2: $t(998) = -72.5$, $p = 0$; Rat 3: $t(998) = -1.96$, $p =$

814 0.05; Rat 4: $t(998) = -53.7$, $p = 2.6 \times 10^{-299}$; Rat 5: $t(998) = -20.0$, $p = 4.1 \times 10^{-75}$). Error
815 bars represent standard error. A single asterisk (*) indicates $p \leq 0.05$, and three asterisks
816 (***) indicate $p < 10^{-74}$.

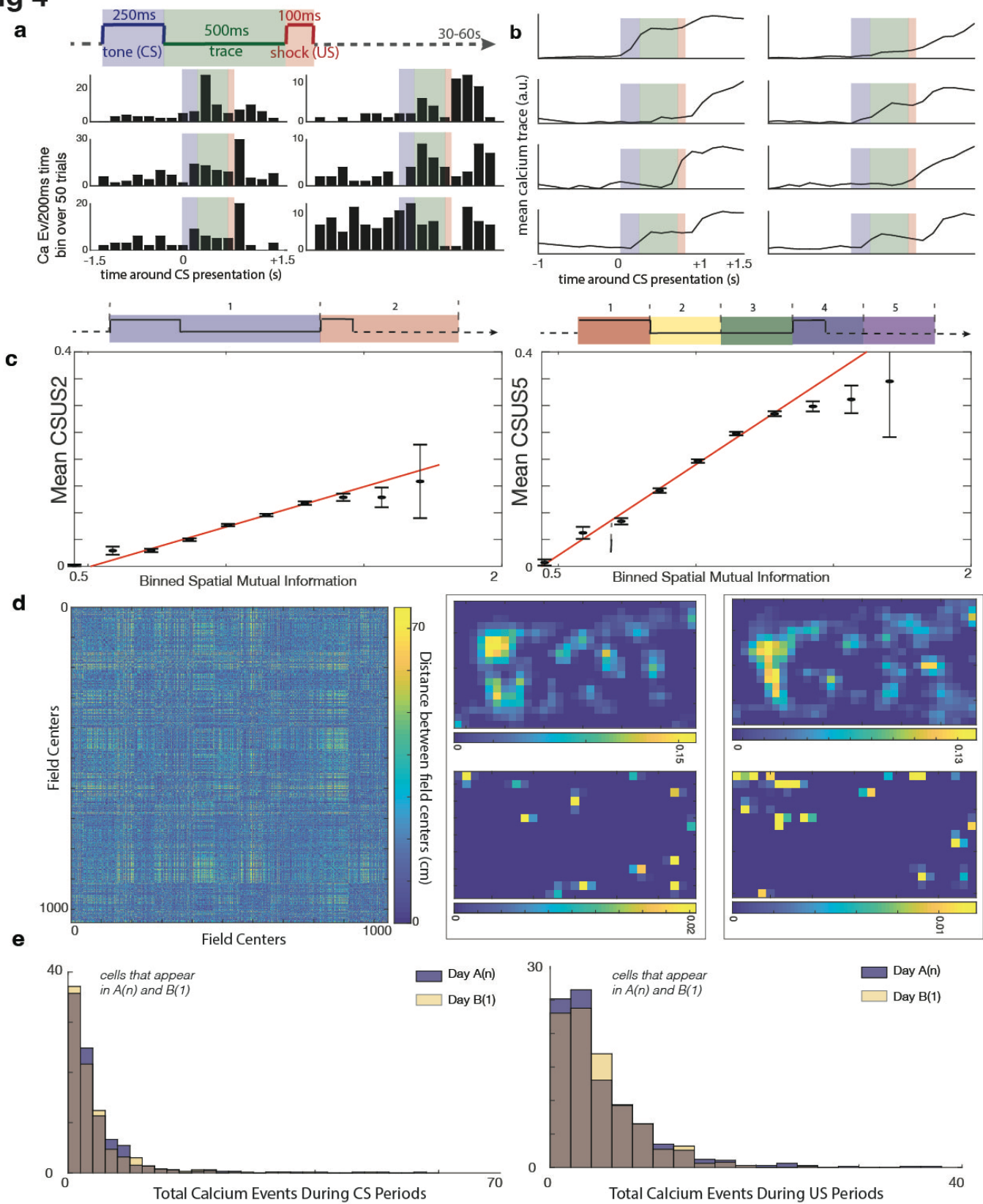
817 **b.** (Top row) Visualization of model performance for decoding animal position in
818 environment A(n). Left: The trained model demonstrated on the training data from
819 session A(n). Middle: The same model applied to held-out trace data (25%) from session
820 A(n). Right: The model applied to predict animal position in session A(n-1). (Bottom
821 row) The same models trained on shuffled position data. Shown here is the model for Rat
822 4, where the model trained on real data significantly outperformed model trained on
823 shuffled data for decoding position in session A(n-1) (500 simulations, $t(998) = -53.7$, $p =$
824 2.6×10^{-299}). For visualization purposes, distance from the corner of the environment is
825 plotted using normalized values in arbitrary units [a.u.].

826 **c.** A model trained on data from session A(n), using cells present in both A(n) and B(1),
827 was applied to environment B(1). The model's predictions were significantly less
828 accurate than those of a model trained on shuffled position data (double-sided t-tests: Rat
829 1: $t(998) = 84.1$, $p = 0$; Rat 2: $t(998) = 18.8$, $p = 7.4 \times 10^{-68}$; Rat 3: $t(998) = 74.7$, $p = 0$;
830 Rat 4: $t(998) = 13.1$, $p = 2.0 \times 10^{-36}$; Rat 5: $t(998) = 154.4$, $p = 0$). Error bars represent
831 standard error. Three asterisks (***) indicate $p < 10^{-35}$.

832 **d.** (Top row) Model trained on position and calcium trace data from session A(n), using
833 cells present in both A(n) and B(1). Left: The model demonstrated on the training data
834 from session A(n). Middle: The same model applied to held-out trace data (25%) from
835 session A(n). Right: The model applied to predict the animal position in session B(1).
836 (Bottom row) The same models trained on shuffled position data. Shown here is the
837 model for Rat 4, where the shuffled model performed significantly better than the model

838 trained on session A(n) for decoding position in session B(1) (500 simulations, $t(998) =$
839 13.1, $p = 2.0 \times 10^{-36}$). For visualization purposes, distance from the corner of the
840 environment is plotted using normalized values in arbitrary units [a.u].
841
842

Fig 4



844 **Figure 4. Identifying CS and US modulation in individual cells**

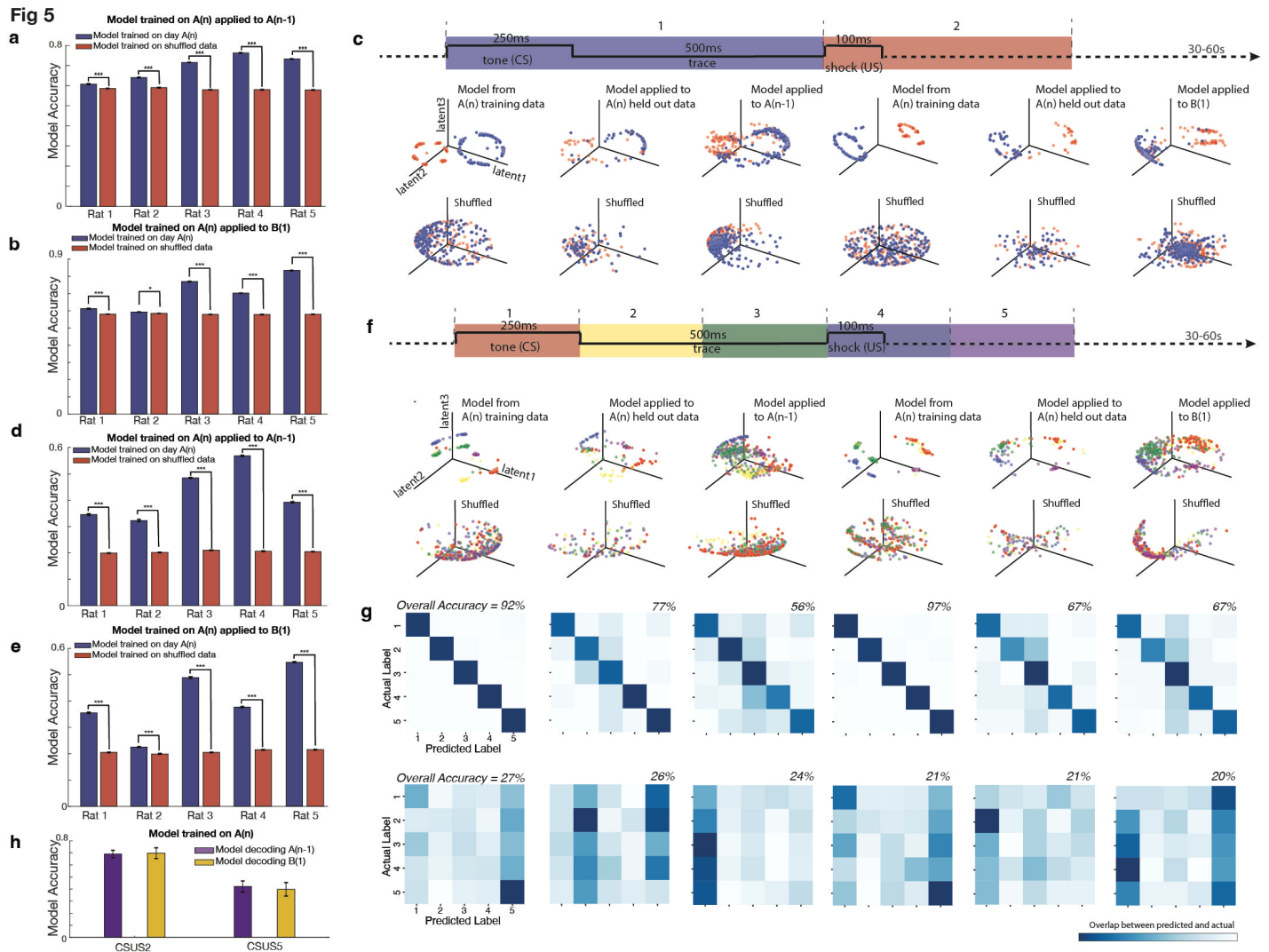
- 845 **a.** Peristimulus time histograms (PSTHs) of six example cells responding to the CS, US,
846 and/or trace period. Bars represent calcium events summed across 50 trials. The
847 shaded regions indicate different stimulus periods: blue (CS), green (trace), and red
848 (US).
- 849 **b.** Mean calcium traces of eight example cells in response to the CS, US, and/or trace
850 period, averaged across 50 trials. Shaded regions are consistent with panel a (a.u. =
851 arbitrary units).
- 852 **c.** Scatter plots illustrating the significant positive correlation between spatial mutual
853 information (MI) and CSUS mutual information (MI). Data points represent binned
854 observations with error bars showing standard errors. The solid red line represents the
855 best fit from a linear regression analysis of the original unbinned dataset. Left: CSUS-
856 MI2 ($r^2 = 0.04$, $p = 2.1 \times 10^{-104}$). Right: CSUS-MI5 ($r^2 = 0.09$, $p = 1.7 \times 10^{-237}$).
- 857 **d.** Mosaic plots showing the odds ratios for cells modulated by spatial and/or CSUS
858 information. Cells were classified as significantly modulated if their mutual
859 information exceeded 95% of shuffled values. Left: Cells with significant spatial
860 modulation had a 1.35 times higher chance of being significantly modulated by
861 CSUS-MI2 compared to cells without spatial modulation (Fisher's exact test, $p =$
862 0.001). Right: Similar results for CSUS-MI5, where cells with significant spatial
863 modulation had a 1.27 times higher chance of being significantly modulated by
864 CSUS-MI5 (Fisher's exact test, $p = 0.002$).
- 865 **e.** Place field remapping during conditioning and non-conditioning periods. (Left) Heat
866 map comparing the spatial distances between place field centers during conditioning
867 (e.g., during CS/US trials) versus non-conditioning periods (e.g., intertrial intervals).

868 Color represents the absolute difference in distances between field centers: regions
869 with minimal color variation (blue) suggest similar place field centers between the
870 two conditions, while more yellow areas represent significant differences in distance
871 (Mantel statistic = 534.58, $p > 0.05$). (Right) Example of two cells showing spatial
872 calcium activity. Top: Heat maps showing calcium event rates during periods of
873 movement but not conditioning (e.g., intertrial intervals). Bottom: Calcium event
874 rates during CS/US conditioning periods. Dark blue signifies the lowest event rate,
875 and yellow represents the highest event rate. These results show that calcium events
876 during trials are not confined to a cell's place field.

877 **f.** Distribution of calcium events during CS (left) and US (right) periods in sessions
878 A(n) (blue) and B(1) (yellow). No significant difference was observed in
879 hippocampal firing during the CS (left) or US (right) periods between environments
880 A and B (CS: two-tailed t-test, $t(1174) = 0.68$, $p > 0.05$; US: two-tailed t-test, $t(1174)$
881 $= 1.20$, $p > 0.05$; KS tests, $p > 0.05$ for both comparisons).

882

883



885

886 **Fig. 5. A model trained in environment A can decode CS and US periods in both**
 887 **environment A and B at above chance levels, including fine-grained temporal decoding.**

888 **a.** A CEBRA model was trained using calcium imaging data and time-stamped CS/US
 889 periods from environment A, using only cells that were recorded in both environments A
 890 and B. The model was used to decode whether the animal was in a CS or US period in
 891 another session in environment A; all models successfully decoded these periods
 892 compared to shuffled data (all double-sided t-tests: Rat 1: $t(998) = 6.7$, $p = 2.5 \times 10^{-11}$;
 893 Rat 2: $t(998) = 16.1$, $p = 7.4 \times 10^{-52}$; Rat 3: $t(998) = 83.5$, $p = 0$; Rat 4: $t(998) = 80.1$, $p =$

894 0; Rat 5: $t(998) = 61.0$, $p = 0$). Bars indicate standard error; significance denoted as *** p
895 $< 10^{-10}$.

896 **b.** The same models from panel a were now applied to environment B; they significantly
897 outperformed chance level (all double-sided t-tests: Rat 1: $t(998) = 10.4$, $p = 2.6 \times 10^{-24}$;
898 Rat 2: $t(998) = 2.7$, $p = 7.6 \times 10^{-3}$; Rat 3: $t(998) = 75.3$, $p = 0$; Rat 4: $t(998) = 63.7$, $p = 0$;
899 Rat 5: $t(998) = 106.3$, $p = 0$). Error bars represent standard error, * $p < 10^{-3}$, *** $p < 10^{-10}$.

900 **c.** (Top row) A CEBRA model trained on CS/US periods, divided into two time bins (data
901 from Rat 4). For the top first three graphs, the model was trained using position and
902 calcium trace data from session A(n), using cells present in both A(n) and A(n-1). First
903 graph: The trained model applied to training data from session A(n). Second graph: The
904 model applied to decode CS/US periods from held-out data (25%) from session A(n).
905 Third graph: The model applied to session A(n-1). For the top last three graphs, the
906 model was trained using position and calcium trace data from session A(n), using cells
907 present in both A(n) and B(1). Fourth graph: The trained model applied to training data
908 from session A(n). Fifth graph: The model applied to decode CS/US periods from held-
909 out data (25%) from session A(n). Sixth graph: The model applied to session B(1).

910 (Bottom row) The same model trained on shuffled data. The model trained on data from
911 session A(n) significantly outperformed the model trained on shuffled data in decoding
912 both session A(n-1) and session B(1) (double-sided t-tests, $t(998) = 83.5$, $p = 0$, and
913 $t(998) = 75.3$, $p = 0$, respectively).

914 **d.** A CEBRA model was trained on data from environment A to decode temporal order
915 within the CS, trace, and US periods split into five divisions, applied to an alternate
916 session in environment A (session A(n-1)). The model significantly outperformed chance
917 (all double-sided t-tests for accuracy: Rat 1: $t(998) = 41.5$, $p = 3.3 \times 10^{-220}$; Rat 2: $t(998)$

918 = 28.7, $p = 7.8 \times 10^{-133}$; Rat 3: $t(998) = 122.6$, $p = 0$; Rat 4: $t(998) = 118.5$, $p = 0$; Rat 5:
919 $t(998) = 62.6$, $p = 0$). Bars indicate standard error; significance denoted as $***p < 10^{-10}$.

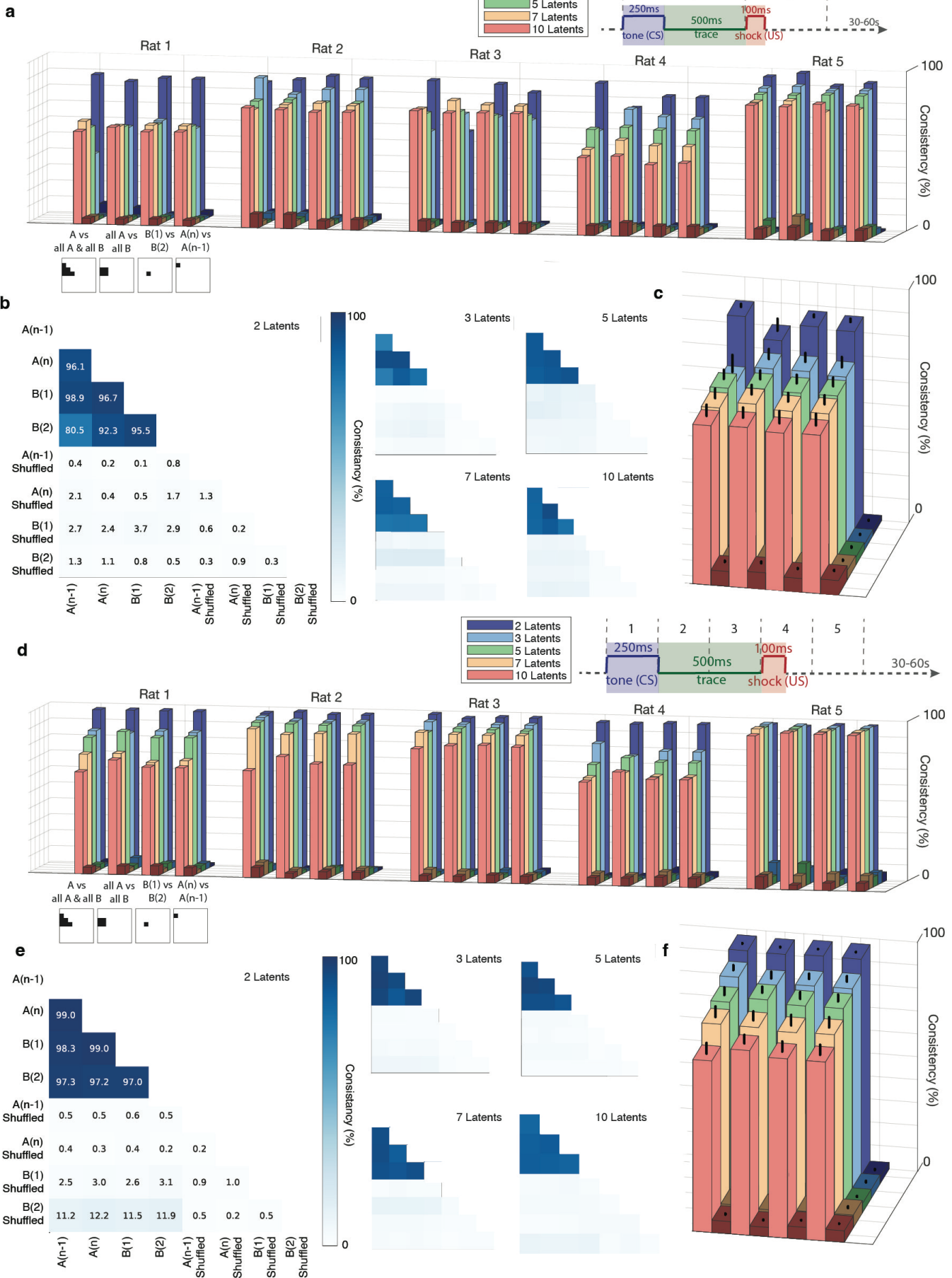
920 **e.** The same five models from panel d were now applied to environment B and
921 outperformed models trained on shuffled data in decoding the temporal aspects of the
922 CS/US periods, indicating that fine-grained temporal encoding is stable across
923 environments (all double-sided t-tests for accuracy: Rat 1: $t(998) = 55.1$, $p = 4.9 \times 10^{-305}$;
924 Rat 2: $t(998) = 9.3$, $p = 1.1 \times 10^{-19}$; Rat 3: $t(998) = 71.4$, $p = 0$; Rat 4: $t(998) = 62.6$, $p =$
925 0 ; Rat 5: $t(998) = 106.2$, $p = 0$). Bars indicate standard error; significance denoted as
926 $***p < 10^{-10}$.

927 **f.** Same analysis as in panel c, but for a CEBRA model trained on CS/US periods split into
928 five time bins. Top: The five divisions of the conditioning period are shown. Data from
929 Rat 3 show that the model trained on session A(n) outperformed models trained on
930 shuffled data when decoding both session A(n-1) and session B(1) (double-sided t-tests,
931 $t(998) = 88.9$, $p = 0$, and $t(998) = 71.4$, $p = 0$, respectively).

932 **g.** Confusion matrices displaying CEBRA decoding of five CS/US time bins, as shown in
933 panel f. Top row: Models trained on data from session A(n). Bottom row: Models trained
934 on shuffled data. Darker colors along the diagonal indicate higher model accuracy.

935 **h.** Model accuracy for decoding sessions A(n-1) and B(1) using a model trained on data
936 from session A(n) with CSUS2 and CSUS5 divisions. For both CSUS2 and CSUS5, a
937 model trained in session A(n) decoded session B(1) with accuracy similar to that
938 achieved when decoding session A(n-1) (CSUS2: double-sided t-test, $t(8) = -0.13$, $p >$
939 0.05 ; CSUS5: $t(8) = 0.32$, $p > 0.05$). Bars represent standard error
940
941

Fig 6



943 **Fig 6. High consistency in neural representations between environments A and B.**

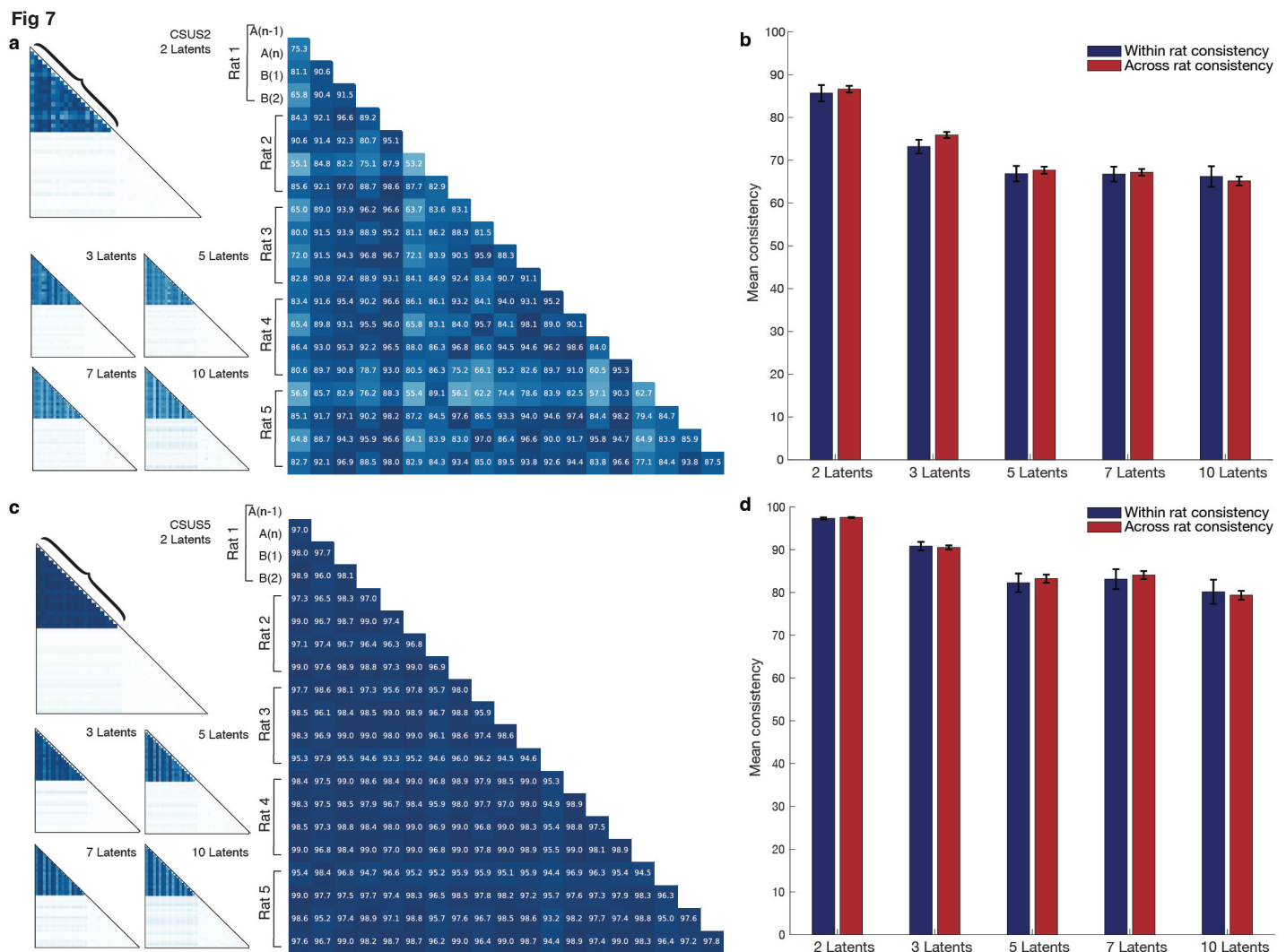
- 944 a. Consistency scores for each rat, calculated with 2, 3, 5, 7, and 10 latents. Lighter bars
945 represent consistency percentage for actual data, while adjacent darker bars represent
946 consistency for shuffled data. The schematic below the x-axis illustrates the data sets
947 included in each comparison (for position and labelling of data sets see figure 6b).
948 For the CSUS2 division of conditioning periods (split into CS and US components),
949 all five rats show significantly higher consistency between environments A and B in
950 the actual data compared to shuffled data. This consistency remains significant with
951 up to 10 latents.
- 952 b. Example consistency measurements from Rat 5 for CSUS2 with 2, 3, 5, 7, and 10
953 latents.
- 954 c. Average consistency scores across all rats for CSUS2. The figure legend follows the
955 format of panel a. Bars represent standard error. Consistency scores for actual data
956 versus shuffled data were significantly different across all latent dimensions (all
957 double-sided t-tests: 2 latents, $p < 1 \times 10^{-5}$; 3 latents, $p < 1 \times 10^{-4}$; 5 latents, $p < 1 \times$
958 10^{-5} ; 7 latents, $p < 1 \times 10^{-5}$; 10 latents, $p < 1 \times 10^{-4}$).
- 959 d. Consistency scores for each rat, as in panel a, but for CSUS5, where the conditioning
960 period is divided into five time bins. All five rats show significantly higher
961 consistency between environments A and B in the actual data compared to shuffled
962 data; this is maintained across latents for up to 10.
- 963 e. Example consistency measurements from Rat 3 for CSUS5 with 2, 3, 5, 7, and 10
964 latents.
- 965 f. Average consistency scores across all rats for CSUS5. The figure legend matches that
966 of panel c. Bars represent standard error. Significant differences between actual and

967 shuffled data were observed for all latent dimensions (all double-sided t-tests: 2
968 latents, $p < 1 \times 10^{-12}$; 3 latents, $p < 1 \times 10^{-7}$; 5 latents, $p < 1 \times 10^{-6}$; 7 latents, $p < 1 \times$
969 10^{-5} ; 10 latents, $p < 1 \times 10^{-5}$).

970

971

972



974

975 **Figure 7. High degree of consistency between the conditioning representations across**
 976 **animals**

977 **a.** Consistency across animals for CSUS2 with 2, 3, 5, 7, and 10 latents. The larger graph
 978 highlights the bracketed area from the graph with two latents.

979 **b.** Conditioning period is divided into 2 time bins (CSUS2): the similarity between models
 980 across animals is not significantly different from the similarity between models for an
 981 individual animal, regardless of the number of latents (2 latents: $t(188) = -0.45$, $p > 0.05$;

982 3 latents: $t(188) = -1.57, p > 0.05$; 5 latents: $t(188) = -0.40, p > 0.05$; 7 latents: $t(188) = -$

983 $0.22, p > 0.05$; 10 latents: $t(188) = 0.40, p > 0.05$). Error bars represent standard error.

984 **c.** Consistency across animals for CSUS5 with 2, 3, 5, 7, and 10 latents. The larger graph

985 highlights the bracketed area from the graph with two latents.

986 **d.** Conditioning period is divided into 5 time bins (CSUS5); the similarity across animal

987 models remains comparable to that for within-animal models, regardless of the number of

988 latents (2 latents: $t(188) = -0.79, p > 0.05$; 3 latents: $t(188) = 0.25, p > 0.05$; 5 latents:

989 $t(188) = -0.42, p > 0.05$; 7 latents: $t(188) = 0.70, p > 0.05$; 10 latents: $t(188) = 0.30, p >$

990 0.05). Error bars represent standard error.

991

992 **Methods**

993 **LEAD CONTACT AND MATERIALS AVAILABILITY**

994 Questions and requests for information should be directed to and will be fulfilled by the
995 Lead Contact, Hannah Wirtshafter (hsw@northwestern.edu). This study did not generate new
996 unique reagents. The data that support the findings of this study are available from the
997 corresponding author.

998

999 **EXPERIMENTAL MODEL AND SUBJECT DETAILS**

1000 All procedures were performed within Northwestern Institutional Animal Care and Use
1001 Committee and NIH guidelines. Five male Long Evans rats (275–325 g) were sourced from
1002 Charles River Laboratories, injected with AAV9-GCaMP8m, implanted with a 2-mm GRIN lens,
1003 and trained and tested on eyeblink conditioning in two apparatuses (Fig. 1). Animals were
1004 individually housed in an animal facility with a 12/12 h light/dark cycle.

1005

1006 **METHOD DETAILS**

1007 **GCaMP7c injection, lens implantation, EMG implantation**

1008 GCaMP8 injection and lens implantation were completed as reported in Wirtshafter and
1009 Disterhoft, 2022 and Wirtshafter and Disterhoft, 2023^{1,2}. Briefly, rats were anesthetized with
1010 isoflurane (induction 4%, maintenance 1-2%) and a craniotomy was performed at stereotaxic
1011 coordinates Bregma AP –4.00mm, ML 3.00mm. 0.06uL of GCaMP8m (obtained from
1012 AddGene, packaged AAV9 of pGP-AAV-syn-jGCaMP8m-WPRE, lot v175525, titer 1.3E+13
1013 GC/mL) was injected over 12 minutes (approximate coordinates Bregma AP –4.00mm, ML
1014 3mm, DV 2.95mm relative to skull); then the syringe was raised 0.2mm and an additional 0.6ul

1015 of GCaMP7 was injected. We repeated this process once more and at slightly different
1016 coordinates in the craniotomy hole, resulting in 4 total injections.

1017 We then aspirated tissue from the craniotomy site using a vacuum pump and 25 gauge
1018 needle. Tissue was aspirated up to and including the horizontal striations of the corpus collosum.
1019 A 2mm GRIN lens (obtained from Go!Foton, CLH lens, 2.00mm diameter, 0.448 pitch, working
1020 distance 0.30mm, 550nm wavelength) was then inserted into the craniotomy hole and cemented
1021 in place using dental acrylic. Animals were given buprenorphine (0.05mg/kg) and 20mL saline,
1022 taken off anesthesia, and allowed to recover in a clean cage placed upon a heat pad.

1023 Six to eight weeks after surgery, animals were again anesthetized with isoflurane and
1024 checked for GCaMP expression. If expression was seen, baseplates were attached using UV-
1025 curing epoxy and dental acrylic. Electrode implantation to record obicularis oculi
1026 electromyographic (EMG) activity occurred in the same surgery as baseplate attachment, as
1027 described previously^{3,4}. Briefly, a connector containing 5 wires was cemented on the front of the
1028 animal's head: 4 wires were implanted directly above the eye in the surrounding muscle (2 for
1029 recording, 2 for electrical stimulation). An additional wire was attached to a connector attached
1030 to a ground screw located above the cerebellum; this screw was implanted during lens
1031 implantation surgery.

1032

1033 **Behavioral environment and training**

1034 Two behavioral apparatuses were used in these experiments: Environment A was a
1035 78.7cm x 50.8cm unscented rectangular enclosure with wire floor and walls and white lighting.
1036 Environment B was a 50.1cm x 34.9cm scented (with two dabs of clove essential oil on opposite
1037 walls) ovular enclosure with white solid floor and walls, and red lighting. Both environments
1038 were located at the same spot in the room relative to external cues (see Figures 1b and S1).

1039 A tether containing a plug to relay the EMG activity and to deliver a shock to the rat's eye
1040 was attached to a the eyeblink connector on the rat's head. The miniscope was plugged into the
1041 cemented baseplate. The miniscope and EMG cords were all attached to a commutator for ease
1042 of animal movement.

1043 The CS was a 250ms, 85dB free-field tone (5ms rise-fall time). The US was a 100ms
1044 shock directed to the left eye. Shock amount varied per session per animal and was calibrated, if
1045 needed, at the end of a training session for the next session's training. Shock level was deemed
1046 appropriate when a shock was met with a firm shake of the animal's head.

1047 The trace interval was 500ms and the intertrial interval (ITI) was randomized between
1048 30s and 60s, with a 45s average. EMG signal output was amplified (5000×) and filtered (100 Hz
1049 to 5 kHz), then digitized at 3 kHz and stored by computer.

1050 A conditioned response (CR) was identified as an increase in integrated EMG activity
1051 that exceeded the baseline mean amplitude by more than four standard deviations, sustained for a
1052 minimum duration of 15ms. Baseline mean amplitude was calculated during the 500ms
1053 preceding CS onset. Additionally, the response had to commence at least 50ms after the
1054 conditioned stimulus (CS) onset and before the unconditioned stimulus (US) onset.

1055 The animal's first exposure to each environment was a 38min exploration session, in
1056 which the animal was able to freely move and explore the environment without any conditioning
1057 (Figure 1a). Animals were then trained in one environment per session, with no more than one
1058 session per day, and were considered to have learned the task after reaching criterion (70% CRs
1059 in 50 trials) on three consecutive training sessions (termed 'criterion sessions') or when the
1060 previous four training sessions averaged over 70% (in this instance, only the final three of those
1061 sessions were considered 'criterion sessions'). Following the last session in environment A, the
1062 animal was given an exploratory session in environment B. The session after that, the animal was

1063 tested on eye blink conditioning in environment B, using the same parameters as used in
1064 environment A.

1065

1066 **Calcium imaging**

1067 Calcium imaging was completed as reported in Wirtshafter and Disterhoft, 2022 and
1068 Wirtshafter and Disterhoft, 2023^{1,2}. Briefly, calcium imaging was done using UCLA V4
1069 Miniscopes^{5,6}, assembled with two 3mm diameter, 6mm FL achromat lens used in the objective
1070 module and one 4mm diameter, 10mm FL achromat lens used in the emission module.

1071

1072 **QUANTIFICATION AND STATISTICAL ANALYSIS**

1073 Means are presented as mean±-standard deviation. All analysis code is available
1074 at https://github.com/hsw28/ca_imaging and <https://github.com/hsw28/Hannahs-CEBRAs>. Code
1075 to create specific figures is also available at the former github repository.

1076

1077 **Position and speed analysis**

1078 Position was sampled by an overhead camera at 30Hz. Position tracking was done post-
1079 recording using DeepLabCut⁷. Position was then converted from pixels to cm. Position was
1080 smoothed using a Gaussian filter with standard deviation of 2cm. Speed was calculated by taking
1081 the hypotenuse of the coordinates one before and after the time of interest.

1082

1083 **Video pre-processing and cell identification**

1084 Video pre-processing and cell identification were performed as reported in Wirtshafter
1085 and Disterhoft, 2022 and Wirtshafter and Disterhoft, 2023^{1,2}. In brief, videos were recorded with
1086 Miniscope software at 15frames/second. Video processing was done using CIATAH software⁸.

1087 Videos were down sampled in space and normalized by subtracting the mean value of each
1088 frame from the frame. Each frame was then normalized using a bandpass FFT filter (70-
1089 100cycles/pixel) and motion corrected to a using TurboReg⁹. Videos were then converted to
1090 relative florescence ($\Delta F/F_0$); F_0 was the mean over the entire video.

1091 Cells were automatically identified using CIATAH⁸ using CNMF-E¹⁰. Images were
1092 filtered with a gaussian kernel of width 2 pixels and neuron diameter was set at a pixel size of 8.
1093 The threshold for merging neurons was set at a calcium trace correlation of 0.65; neurons were
1094 merged if their distances were smaller than 4 pixels and they had highly correlated spatial shapes
1095 (correlation>0.8) and small temporal correlations (correlation <0.4).

1096 In vivo calcium imaging involves detecting changes in intracellular calcium levels, which
1097 serve as proxies for neuronal activity. Calcium events refer to transient increases in calcium
1098 concentration above a threshold level; these crossings putatively correspond to spikes in neuronal
1099 firing. These events typically appear as peaks in the data and indicate an active response from the
1100 neuron. Calcium traces are continuous recordings of calcium levels over time. Thus, calcium
1101 events highlight specific neuronal activations, while calcium traces provide a full temporal
1102 picture of these activations together with baseline activity.

1103 All cells identified using CNMF-E were then scored as neurons or not by a human scorer.
1104 Scoring was also done within CIATAH software in a Matlab GUI. Scoring was done while
1105 visualizing and considering a calcium activity trace, average waveform, a montage of the
1106 candidate cell's Ca²⁺ events, and a maximum projection of all cells on which the candidate cell
1107 was highlighted. The relative florescence ($\Delta F/F_0$) local maxima of each identified cell were
1108 considered calcium event times.

1109

1110 **Cell cross registration across sessions and within session**

1111 Validation and registration were completed as documented in Wirtshafter and Disterhoft².
1112 Briefly, videos underwent five rounds of registration using Turboreg image rotation⁹ with the
1113 CIATAH software^{8,11}. Background noise, axons, and dendrites were removed using an image
1114 binarization threshold of 40% of the images' maximum value. Cells were matched across
1115 sessions using a distance threshold of a maximum of five pixels, with a minimum 2-D correlation
1116 coefficient of 0.5. Sessions were aligned to session A(n), the last session in environment A.

1117

1118 **Place cell identification and computing spatial mutual information**

1119 Place cells were identified using mutual information computed when the animals were
1120 running at speeds greater than or equal to 4cm/s. MI was computed for all cells; there was no
1121 calcium event rate criterion for included cells. To be considered significant, the computed mutual
1122 information (MI) must be greater than 95% of MI scores computed 500 times from shuffled
1123 positions¹². To compute the MI for each cell, the training environments were divided into 2.5cm
1124 x 2.5cm bins. The calcium event rate of each cell and the occupancy of the animal were found
1125 for each bin. Rate and occupancy were smoothed with a Gaussian kernel with filter width of 3cm
1126 and Sigma of 0.5cm. Mutual information was computed during periods of movement as
1127 follows^{2,12,13}:

1128

1129

1130

1131

$$p = \frac{P_s}{P_o}$$
$$M_s = \sum P_s$$
$$M_o = \sum P_o$$
$$MI = \sum p * \log_2\left(\frac{p}{M_s * M_o}\right)$$

1132

where:

1133

P_s = calcium event probability in each bin

1134

P_o = occupancy probability at each bin

1135

1136 Mutual information using calcium traces was computed as above, except instead of P_s
1137 being calcium event probability per bin, the value of P_s was the average value of calcium trace in
1138 the bin.

1139 We computed MI using both calcium events and calcium trace data. There was no
1140 significant difference between the number of place cells detected using calcium event data and
1141 calcium trace data, (paired t-test $t(24)=1.01$, $p>0.05$). Note that all place cell and place field
1142 measurements are presented with conditioning periods included, as the animal was frequently
1143 moving during conditioning periods. We also computed results while excluding conditioning
1144 periods and found no significant differences.

1145

1146 **Computing CSUS mutual information**

1147 The computation of CSUS mutual information was very similarly to that for spatial
1148 mutual information. A 1.3 second period beginning at the start of the CS tone was either divided
1149 into 2 bins (CSUS-MI2) or 5 bins (CSUS-MI5) (Fig. 3c-3d). Mutual information was then
1150 computed using the following:

$$\begin{aligned} 1151 \quad p &= \frac{P_s}{P_o} \\ 1152 \quad M_s &= \sum P_s \\ 1153 \quad M_o &= \sum P_o \\ 1154 \quad MI &= \sum p * \log_2\left(\frac{p}{M_s * M_o}\right) \end{aligned}$$

1155 Where:

1156 P_s = calcium event probability in each CSUS bin
1157 P_o = probability of individual CSUS occurring out of all CSUS bins

1158

1159

1160 Mutual information using calcium traces was computed as above, except that P_s did not
1161 represent the calcium event probability per bin, but the average value of calcium trace within the
1162 bin.

1163

1164 **Remapping quantification**

1165 The place cell center was defined as the occupancy-normalized location with maximum
1166 number of calcium events while the animal was moving at 5cm/s or faster. Position was binned
1167 into 2.5cm square bins. The place cell centers at environments A and B, as well as at
1168 environment A across days and at environment B across days, were used to align each
1169 environment across days, as well as to align environment A to environment B.

1170 Population vector correlation was calculated between two environments using calcium
1171 event data. Neurons present in both datasets (such as sessions A(n) and A(n-1), or A(n) and B(1))
1172 were identified and their calcium event times were converted to rates using 0.75 second binning.
1173 These firing rates were then normalized using z-score normalization across each neuron's activity
1174 across time. The mean calcium event rate for each neuron in each environment was then
1175 computed. The correlation among population vectors of firing rates in the two environments was
1176 computed:

1177

$$1178 \text{ population vector correlation} = \frac{\sum_{i=1}^N (r_{\{i,A\}} - \overline{\{r\}}_A) (r_{\{i,B\}} - \overline{\{r\}}_B)}{\sqrt{\sum_{i=1}^N (r_{\{i,A\}} - \overline{\{r\}}_A)^2} \sqrt{\sum_{i=1}^N (r_{\{i,B\}} - \overline{\{r\}}_B)^2}}$$

1179

1180

1181 *Where:*

1182 $r_{\{i,A\}}$ and $r_{\{i,B\}}$ = firing rates of neuron i in environments A and B

1183 $\overline{\{r\}}_A$ and $\overline{\{r\}}_B$ = mean firing rates across neurons in environments A and B

1184 The factors in the denominator correspond to the standard deviation of the components of
1185 each population vector relative to their mean, computed in each environment.

1186

1187 **Use of CEBRA versus alternative methods**

1188 We explored multiple different methods before settling on the use of CEBRA for this
1189 study. A short summary of each tested method can be found below:

1190

1191 • **Principal Component Analysis (PCA)**¹⁴: Principal component analysis (PCA) is a
1192 statistical method used to reduce the dimensionality of data while retaining as much
1193 variability as possible. This linear technique identifies the axes (principal components) in
1194 the dataset that maximize variance. The first principal component explains the most
1195 variance, the second explains the second most, and so on. Principal components are
1196 combinations of original features and may not always have clear or intuitive meanings. In
1197 agreement with previous hippocampal data¹⁵, PCA required upwards of 15-25
1198 components to capture 95% of the variance of the data. In addition, across and within all
1199 sessions and representations (spatial and task representations), the manifolds spanned by
1200 the largest PCs remained highly similar, with small principal angles in pairwise
1201 comparisons. This similarity in the orientation of the leading subspaces suggested that
1202 PCA did not distinguish between spatial or behavioral components of the task (Figure
1203 S5).

1204 • **Independent Component Analysis (ICA)**¹⁶: Independent Component Analysis (ICA) is
1205 a computational technique used to separate a multivariate signal into additive,
1206 independent components. ICA operates under the assumption that observed data are
1207 linear mixtures of underlying, independent sources. It aims to find a linear transformation
1208 that maximizes the statistical independence of the estimated components. We found that
1209 ICA embeddings were unstable throughout the length of the recordings, and also did not
1210 clearly map onto behavioral states (Figure S6).

1211 • **Isomap**¹⁷: Isomap is a manifold learning technique that seeks to capture the intrinsic
1212 geometric structure of data. Isomap is useful when linear methods like PCA cannot
1213 capture the intrinsic structure of the data, as it preserves the geodesic (curved) distances

1214 in the reduced dimensionality space. Unlike linear methods such as PCA, Isomap can
1215 capture nonlinear relationships in the data. Interestingly, using Isomap, only about 5
1216 neural modes were required to achieve a residual variance of 5-10%. However, the
1217 embedding shape did not relate to any discernable property of neural data or behavior
1218 (Figure S7). Dimensionality reduction was achieved, but the resulting representations
1219 were not interpretable (Figure S7).

1220 • **MIND**^{15,18}: MIND is a decoding method designed for integrating multiple data modalities
1221 to predict various features, particularly sensory and motor functions. MIND uses
1222 recurrent neural networks whose hidden variables provide a memory mechanism for
1223 remembering previous inputs; this approach is particularly apt for the analysis of time
1224 series data such as neural recordings. While MIND was very robust at distinguishing the
1225 different environments, it was not equipped to handle relatively short signals separated in
1226 time, such as the conditioning trials separated by intertrial intervals. Our analyses using
1227 MIND resulted in poor and unstable embeddings that could not be analyzed (Figure S8).

1228 CEBRA¹⁹ was chosen for this project for its ability to capture nonlinear relationships in the data
1229 and to create stable embeddings over short and long time periods. Additionally, spatial
1230 separations of components were well isolated and correlated well with observed behaviors.

1231

1232 **Use of CEBRA for position decoding**

1233 Optimal parameters for decoding the position of each animal from neural activity were
1234 determined using an extensive grid search across learning rate, temperature, and number of
1235 iterations (Figure S9). Models created to compare different sessions, such as a model trained on
1236 data from session A(n) used to decode session B(1), were only trained on cells that occurred in
1237 both sessions. Models were trained on spike traces of these cells, labeled with the animal's (X,Y)

1238 position. In all cases, 75% of data was used to train the model while 25% of data was held out for
1239 verification. All models were run 500 times. Optimal embeddings were determined based on the
1240 minimum median absolute error between the predicted and true positions. The optimal
1241 parameters for each rat are as follows:

	Rat 1	Rat 2	Rat 3	Rat 4	Rat 5
Model Architecture	'Offset10-model'				
Batch size	512				
Learning rate	5.5×10^{-5}	6.625×10^{-4}	5.5×10^{-4}	1.0×10^{-3}	1.0×10^{-3}
Temperature mode	'Auto'				
Minimum temperature	No minimum	1.5	0.95	1.0×10^{-9}	No minimum
Output dimensions (# of latents)	3				
Max iterations	25000	8000	26500	30000	18000
Distance	'Cosine'				
Conditional	'Time delta'				
Number of hidden units	32				
Time offsets	1				

1242

1243 The number of output dimensions was chosen based on the fewest number of dimensions under
1244 which all 5 models consistently outperformed shuffled data for both position and conditioning
1245 decoding (Figure S10-12).

1246

1247 **Use of CEBRA for conditioning decoding**

1248 As in position decoding, the optimal parameters for decoding conditioning were
1249 determined for each animal using an extensive grid search across learning rate, temperature, and
1250 number of iterations (Figure S11). Models created to compare different sessions of neural
1251 activity, such as a model trained on data from session A(n) used to decode session B(1), were

1252 only trained on cells that occurred in both sessions. Models were trained on spike traces of these
1253 cells, with labels corresponding to the CSUS bin during which the signal occurred (either one out
1254 of 2 bins or out of 5 bins, see Figures 3c-d). In all cases, 75% of data was used to train the model
1255 while 25% of data was held out for verification. All models were run 500 times. Optimal
1256 embeddings were determined based on the percent of correctly binned time points. The optimal
1257 parameters for each rat are as follows:

1258

	Rat 1	Rat 2	Rat 3	Rat 4	Rat 5
Model Architecture	'Offset10-model'				
Batch size	512				
Learning rate	3.5×10^{-3}	7.0×10^{-3}	3.5×10^{-3}	7.5×10^{-3}	9.5×10^{-3}
Temperature mode	'Constant'	'Constant'	'Auto'	'Constant'	'Constant'
Minimum temperature	2.33	1.75	1.67	1.67	2.66
Output dimensions (# of latents)	3				
Max iterations	50000	7500	20000	18000	25000
Distance	'Euclidian'	'Cosine'	'Cosine'	'Euclidian'	'Cosine'
Conditional	'Time delta'				
Number of hidden units	32				
Time offsets	1				

1259

1260 The number of output dimension was chosen based on the fewest number of dimensions
1261 under which all 5 models consistently outperformed shuffled data for both position and
1262 conditioning decoding (Figure S10-12). The parameters listed above were used for decoding into
1263 2 or 5 bins, including the use of 3 output dimensions (# of latents).

1264 The accuracy of results was computed from the entries in the confusion matrix:

1265

1266

1267

$$Accuracy = \frac{\text{Sum of number of diagonal (correct) elements}}{\text{Sum of number of total elements}}$$

1268 Precision was calculated for each class i , $1 \leq i \leq n$, where n is the number of classes:
1269

$$1270 \quad \text{Precision}_i = \frac{(TP_i)}{TP_i + FP_i}$$

1271 where:

1272 $TP = \text{true positives}$

1273 $FP = \text{false positives}$

1274

1275 The global precision is given by the average:

$$1276 \quad \text{Precision} = \frac{1}{n} \sum_{i=1}^n \text{Precision}_i$$

1277

1278

1279 Recall, also known as sensitivity, was calculated for each class i , $1 \leq i \leq n$, where n is the

1280 number of classes:

1281

$$1282 \quad \text{Recall}_i = \frac{(TP_i)}{TP_i + FN_i}$$

1283

1284 where:

1285 $TP = \text{true positives}$

1286 $FN = \text{false negatives}$

1287

1288 The global recall is given by the average:

1289

$$1290 \quad \text{Recall} = \frac{1}{n} \sum_{i=1}^n \text{Recall}_i$$

1291

1292 The F1 score was calculated for each class i , $1 \leq i \leq n$, where n is the number of classes:

1293

$$1294 \quad F1_i = 2 * \frac{\text{Precision}_i * \text{Recall}_i}{\text{Precision}_i + \text{Recall}_i}$$

1295

1296 The global F1 score is given by the average:

1297

$$1298 \quad F1 = \frac{1}{n} \sum_{i=1}^n F1_i$$

1299

1300

1301 The area under the receiver operating characteristic (ROC) curve was calculated for each class i ,

1302 $1 \leq i \leq n$, where n is the number of classes:

1303

1304

$$AUC_i = roc_auc_score(y_{true-bin}[:, i], y_{pred-prob}[:, i])$$

1305

1306 The global value is given by the average:

1307

1308

$$ROC\ AUC = \frac{1}{n} \sum_{i=1}^n AUC_i$$

1309

1310

where:

1311

$y_{true-bin} = \text{binarized true labels}$

1312

$y_{pred-prob} = \text{predicted probabilities for each class}$

1313

1314 **Model consistency**

1315

Model consistency was computed using a built-in CEBRA function which relies on the

1316

function ‘sklearn.metrics.consistency_score’²⁰. The function compares the embeddings from

1317

different models by calculating pairwise consistency scores. This comparison involves

1318

measuring the similarity of the embeddings using statistical metrics; i.e. this metric calculates

1319

how similar a model’s labels are for similar instances in the data set.

1320

To determine consistency between environments and across animals, the data was fit to

1321

each model 20 times. The model with the lowest loss was selected and compared to other models

1322

with the lowest loss. Models were created using each individual animal’s optimal parameters

1323

(see above).

1324

1325

1326 **Acknowledgements:** This work was supported by an NIA T32 (T32-AG020506/AG/NIA), an
1327 NIA R37 (R37-AG008796/AG/NIA), an NINDS R01 (R01 NS113804/NS/NINDS), and a K99
1328 award (K99 MH135062).

1329
1330 This research was supported in part through the computational resources and staff assistance
1331 provided by the Quest high performance computing facility at Northwestern University, which is
1332 jointly supported by the Office of the Provost, the Office for Research, and Northwestern
1333 University Information Technology.

1334
1335 We would like to thank all members of the Disterhoft lab, especially Mackenzie Kneisly. We
1336 would like to thank the following individuals for their assistance with CEBRA: Mackenzie
1337 Mathis and Steffen Schneider. And additional thank you to David Wirtshafter for his feedback.

1338
1339
1340 **Author contributions:** Investigation, H.S.W.; Formal Analysis, H.S.W.; Writing –Original
1341 Draft, H.S.W.; Writing – Review & Editing, H.S.W., S.A.S., J.F.D.; Funding: H.S.W, J.F.D.,
1342 Supervision, S.A.S., J.F.D.

1343
1344 **Declaration of interests:** The authors declare no competing interests.

1345

1346 **Additional Information**

1347 Supplementary Information is available for this paper.

1348 Correspondence and requests for materials should be addressed to Hannah S

1349 Wirtshafter, hsw@northwestern.edu .

1350 Reprints and permissions information is available at www.nature.com/reprints.

1351

1352

1353 **Supplementary figures**

1354

Figure S1

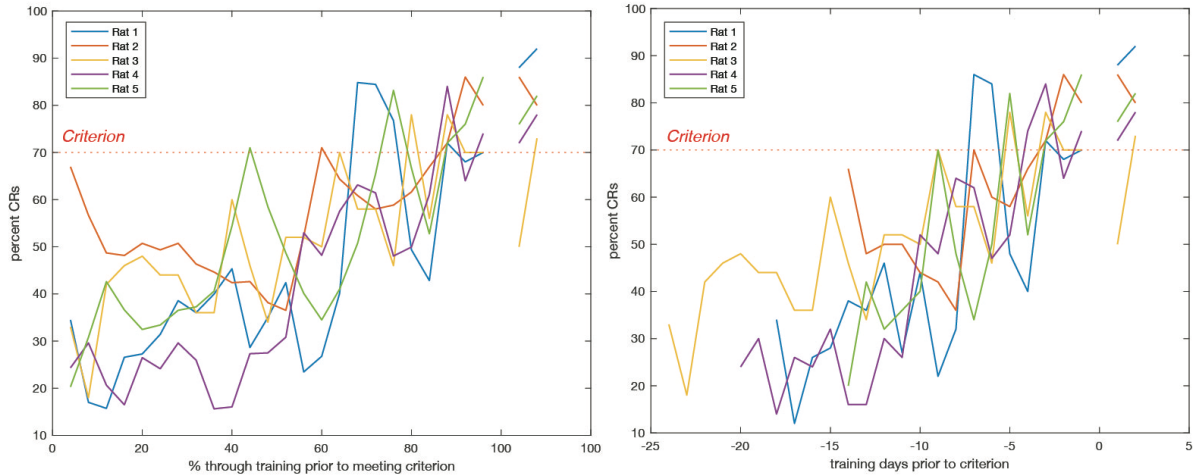


1355

1356 **Figure S1. Photos of testing chambers.**

1357 Photos of testing chambers. Top: Environment A, an unscented rectangular enclosure with wire
1358 floor and walls, and white lighting. Bottom: Environment B, a scented oval enclosure with
1359 white solid floor and walls, and red lighting. Both environments were located at the same spot in
1360 the room relative to external cues. The door to the chamber was closed during testing, to
1361 accentuate the distinction between the white and red lighting.

Figure S2

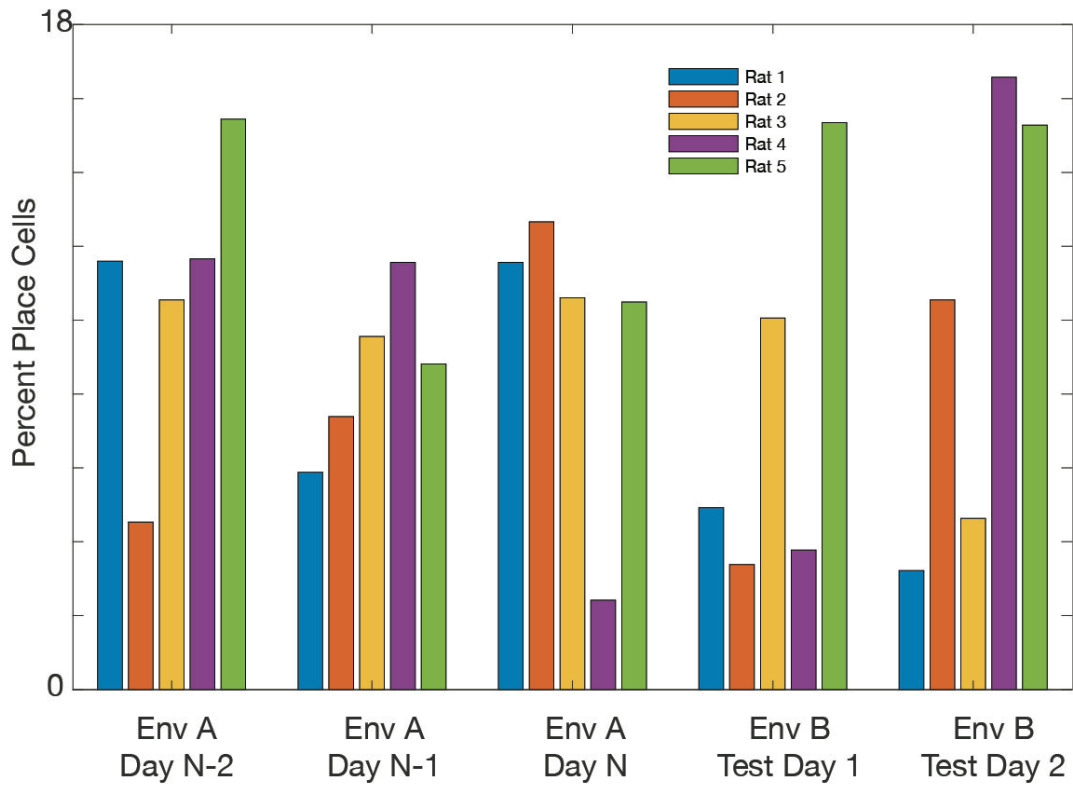


1362

1363 **Figure S2. Learning curves for the five rats.**

1364 Substantial variability in the number of sessions required to learn the task; average number of
1365 sessions was 20 ± 4.2 (including the criterion sessions). The fastest learners (2 rats) reached
1366 criterion after 14 sessions, while the slowest rat required 24 sessions to reach criterion.

Figure S3

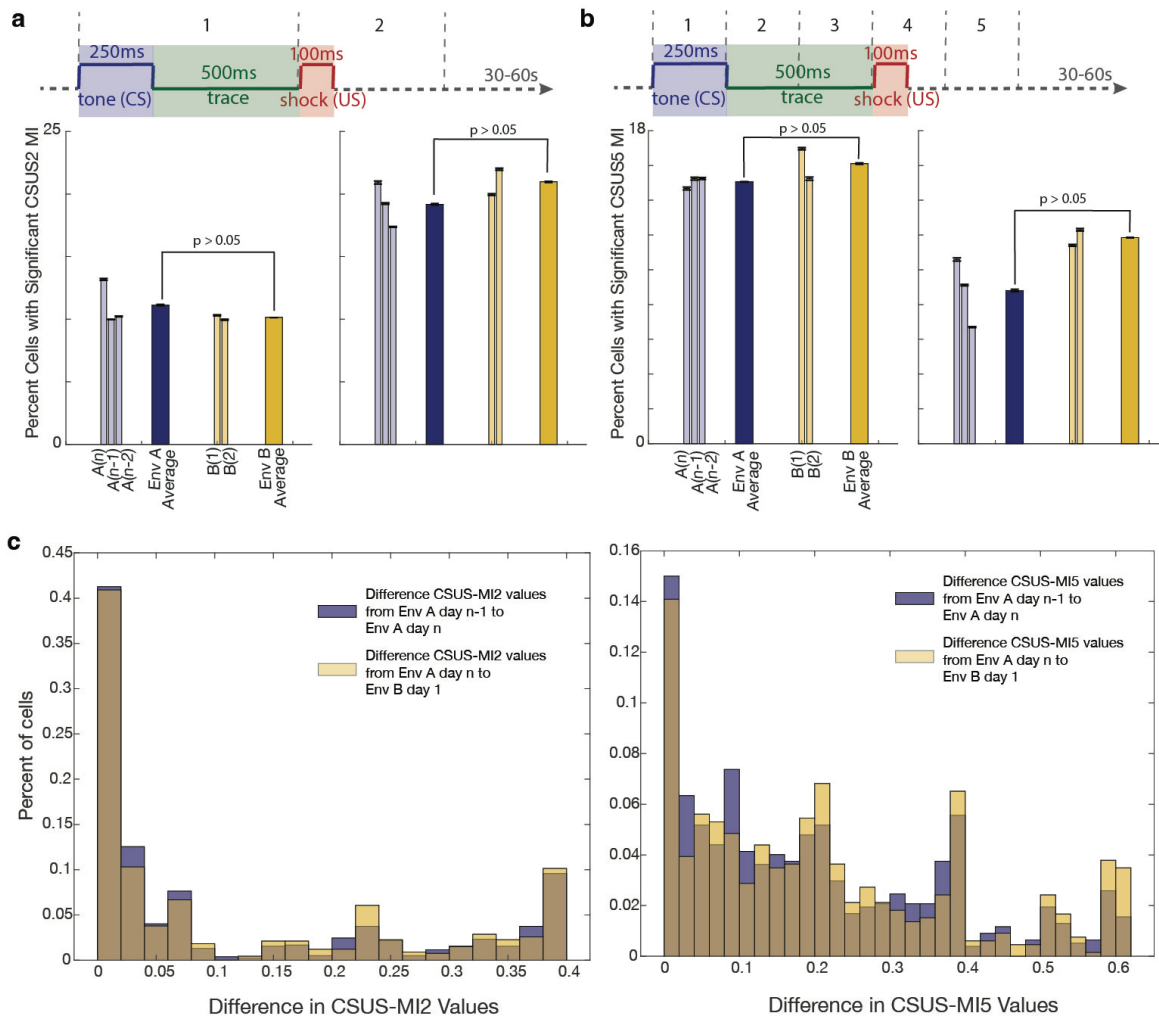


1367

1368 **Figure S3. Percent of place cells by session for each animal.**

1369 The percentage of cells classified as place cells for each session and each animal

Figure S4



1370

1371 **Figure S4. CSUS-MI2 and CSUS-MI5 differences between sessions.**

1372 **a.** The trial period was divided into two segments: the CS and trace period (750 ms) and the
 1373 US and post-US period (500 ms). Mutual information (MI) was calculated for cells based
 1374 on these two periods and compared to shuffled data, where period IDs were shuffled 500
 1375 times across all trials. Left: Using calcium event data, we found that $10.7\% \pm 4.9\%$ of
 1376 cells contained significant CSUS information related to whether the animal was in a CS
 1377 or US period. Right: Using calcium traces, $19.9\% \pm 8.2\%$ of cells contained significant
 1378 information distinguishing the CS from the US period. No significant differences in

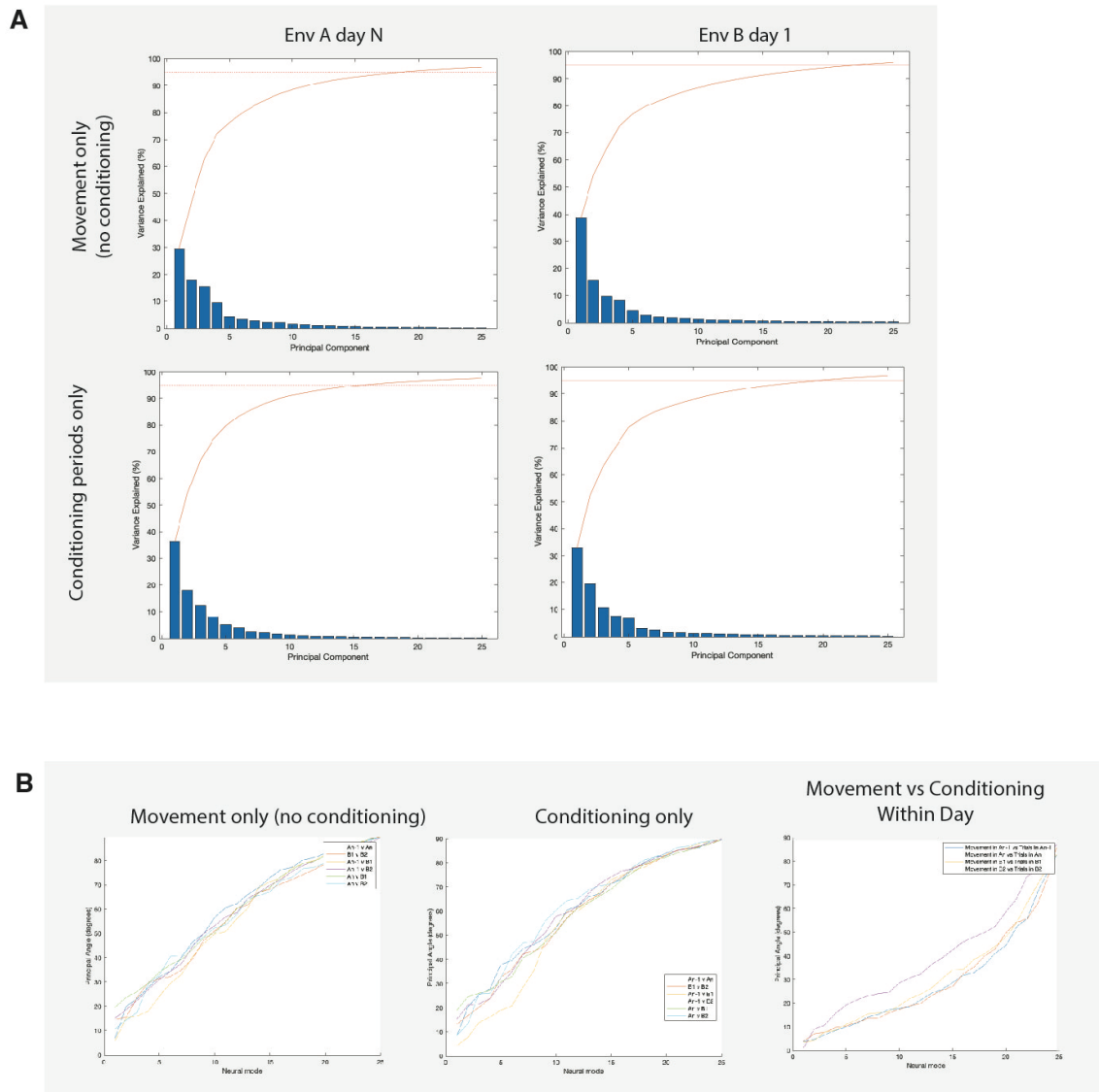
1379 CSUS-MI were observed between environments A and B (double-sided t-tests, calcium
1380 events: $t(23) = 0.48$, $p > 0.05$; calcium traces: $t(23) = -0.52$, $p > 0.05$).

1381 **b.** The trial period was divided into five equal segments, each 250 ms. MI was calculated
1382 for each cell based on these five periods. We compared the observed values to those
1383 obtained after shuffling period IDs 500 times. Left: Using calcium event data, $15.5\% \pm$
1384 7.8% of cells contained significant information distinguishing the five periods, compared
1385 to $10.0\% \pm 7.8\%$ when using calcium trace data. No significant differences in these MI
1386 metrics were found between environments A and B (double-sided t-tests, calcium events:
1387 $t(23) = -0.32$, $p > 0.05$; calcium traces: $t(23) = -1.1$, $p > 0.05$).

1388 **c.** Left: There was no significant difference in CSUS-MI2 values when comparing session
1389 A(n) to session A(n-1) versus session A(n) to session B(1) (Wilcoxon rank sum test: $p >$
1390 0.05 ; double-sided t-test: $t(1431) = 0.86$, $p > 0.05$). Right: A small but significant
1391 difference was observed in CSUS-MI5 when comparing session A(n) to session A(n-1)
1392 versus session A(n) to session B(1) (Wilcoxon rank sum test: $p = 0.049$; double-sided t-
1393 test: $t(1431) = -2.2$, $p = 0.03$).

1394

Figure S5

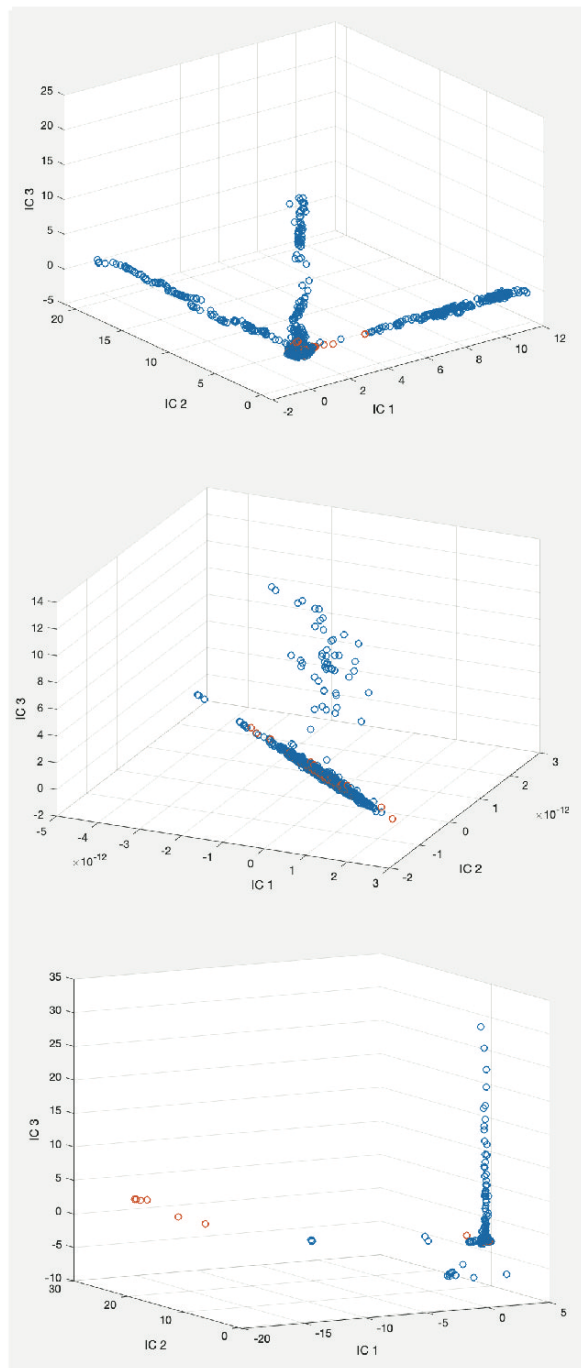


1395

1396 **Figure S5. PCA computations for session A(n) and session B(1).**

1397 Only cells present in both sessions were used. Principal component analysis (PCA) revealed that
1398 approximately 15-25 principal components (PCs) are needed to account for 95% of the variance
1399 in the data. When using the complete cell population (not shown), more than 25 PCs are required
1400 to achieve the same variance. Across and within all sessions and representations (spatial and
1401 task), the principal angles between manifolds remain highly similar.

Figure S6



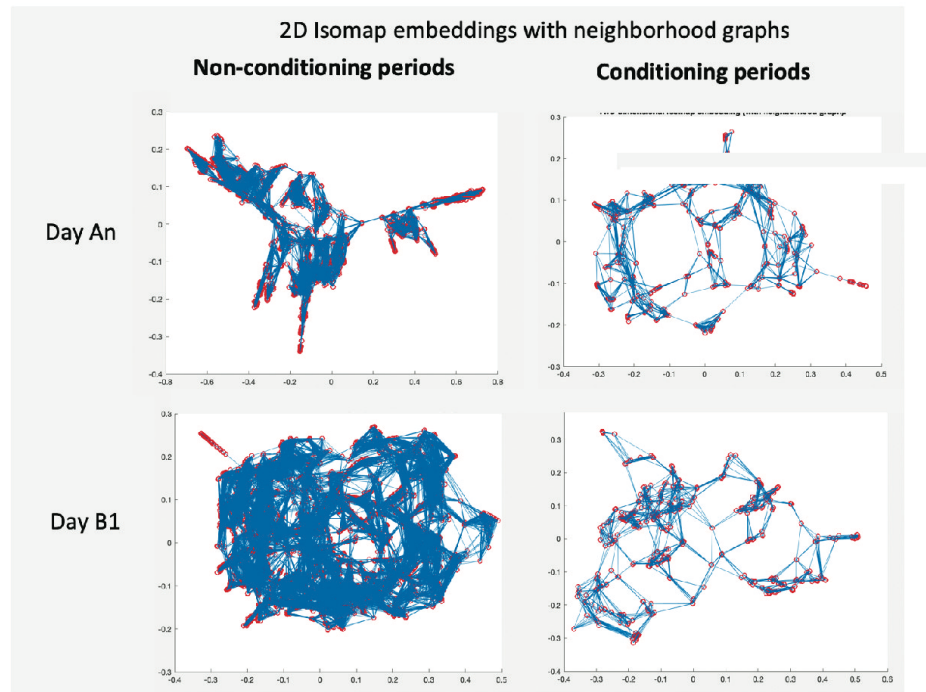
1402

1403 **Figure S6. ICA computations across different segments of a session.**

1404 Top: Independent component analysis (ICA) was for data over an entire session, using three
1405 independent components (ICs). Blue dots represent non-trial times, while red dots represent trial
1406 times. Middle: ICA computed over the last two-thirds of the same session shows variability in

1407 ICs across segments within a session. Bottom: ICA computed over the second half of the session
1408 shows additional variability in the results of the analysis depending on how the session is
1409 divided. These results indicate that independent components are highly variable over the course
1410 of one session and are sensitive to how the session is partitioned.
1411

Figure S7

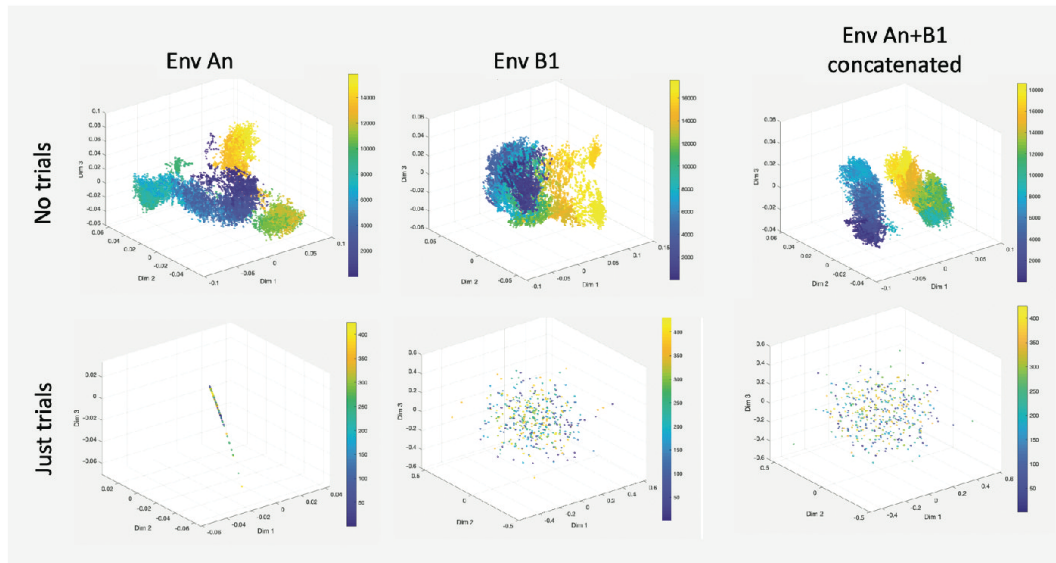


1412

1413 **Figure S7. Isomap computations for session A(n) and session B(1).**

1414 Isomap computations suggest that approximately five neural modes are sufficient to achieve a
1415 residual variance of 5-10%. However, the shape of the Isomap embedding does not correlate
1416 with any discernable properties of neural activity or behavior, suggesting limited interpretability
1417 of the embedding structure.

Figure S8



1418

1419 **Figure S8. MIND outputs for sessions A(n), B(1), and concatenated sessions.**

1420 Top row: MIND embeddings during movement, excluding trial periods, with color bars

1421 representing frames. The temporal structure of the data is well captured, with clear separation

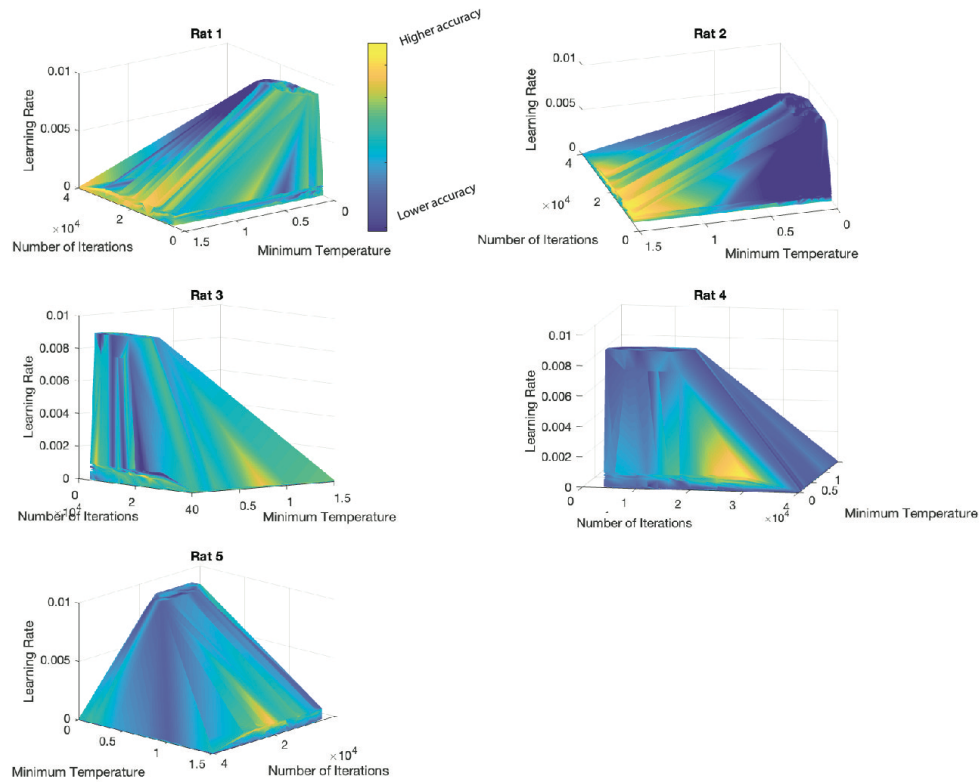
1422 between A(n) and B(1). Bottom row: MIND embeddings during conditioning periods are highly

1423 unstable. Small changes in parameters result in substantial shifts in the embedding structure,

1424 transitioning from a linear structure (left) to an undefined, unstable cloud (middle and right).

1425

Figure S9

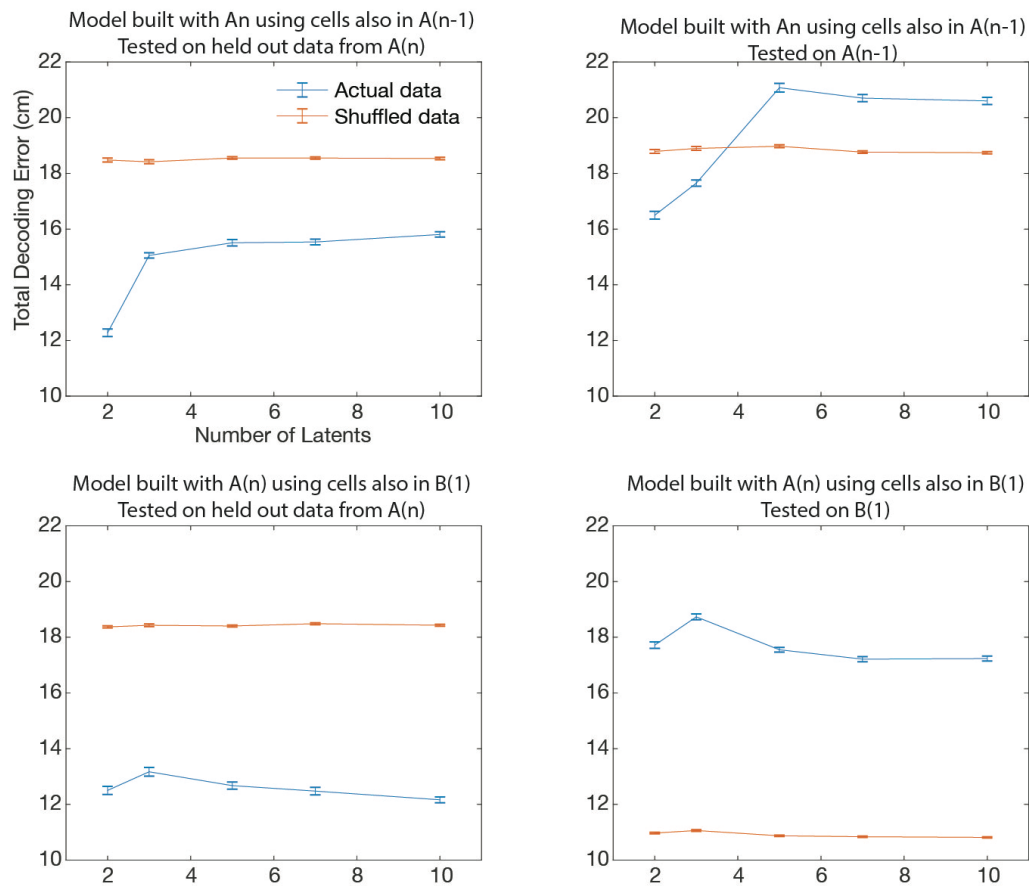


1426

1427 **Figure S9. Grid search over decoding parameters for position.**

1428 A grid search was performed over three parameters: minimum temperature, learning rate, and
1429 number of iterations, for decoding position. Models were trained using cells from session A(n)
1430 that also appeared in session A(n-1). The figure shows decoding accuracy for session A(n-1)
1431 using the models trained on data from session A(n). Yellow areas indicate higher decoding
1432 accuracy.

Figure S10



1433

1434 **Figure S10. Position decoding error as a function of the number of latents (Rat 5).**

1435 This figure shows the decoding error for position as the number of latents increases. Left panels:

1436 model trained on data from $A(n)$, tested on held out data from $A(n)$. Upper left panel: As the

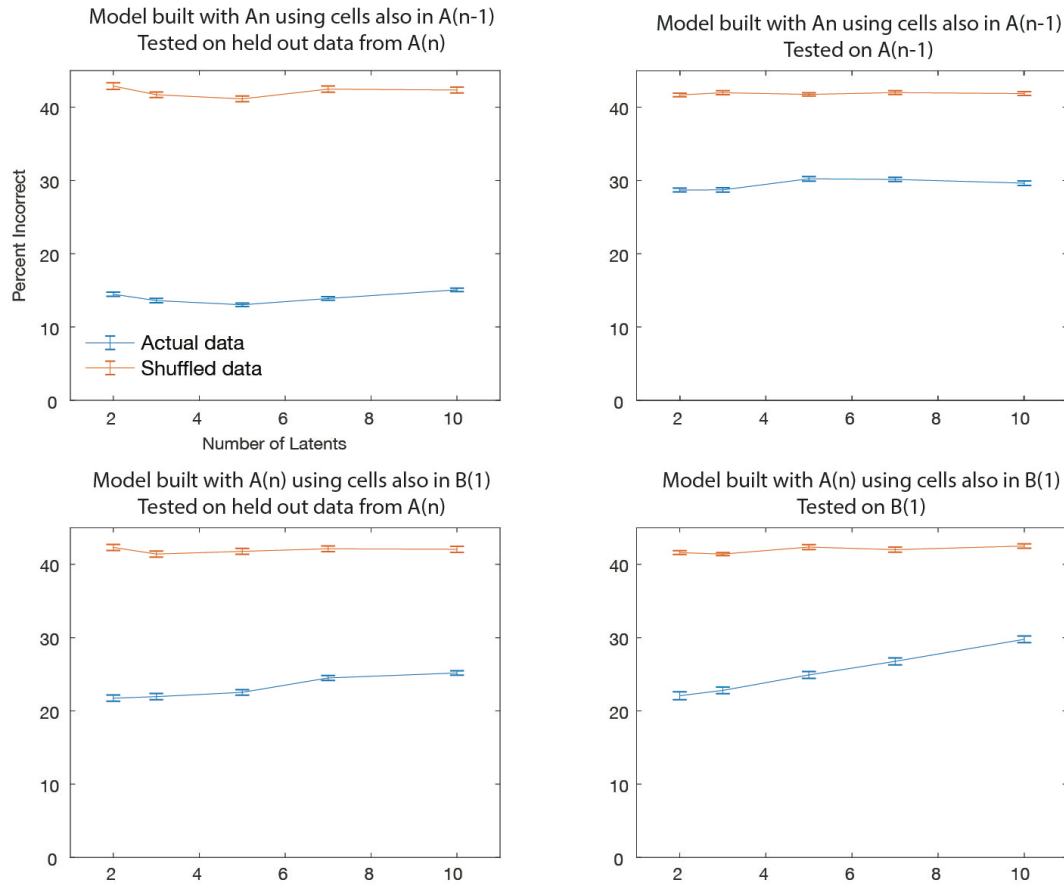
1437 number of latents increases, the model's ability to decode a different session within the same

1438 environment decreases. This effect is not consistent across all rats; see lower left panel. Right

1439 panels: model trained on data from $A(n)$, tested on $A(n-1)$ (top) or $B(1)$ (bottom). Performance is

1440 particularly bad when the model is tested on a different environment (lower right panel).

Figure S11

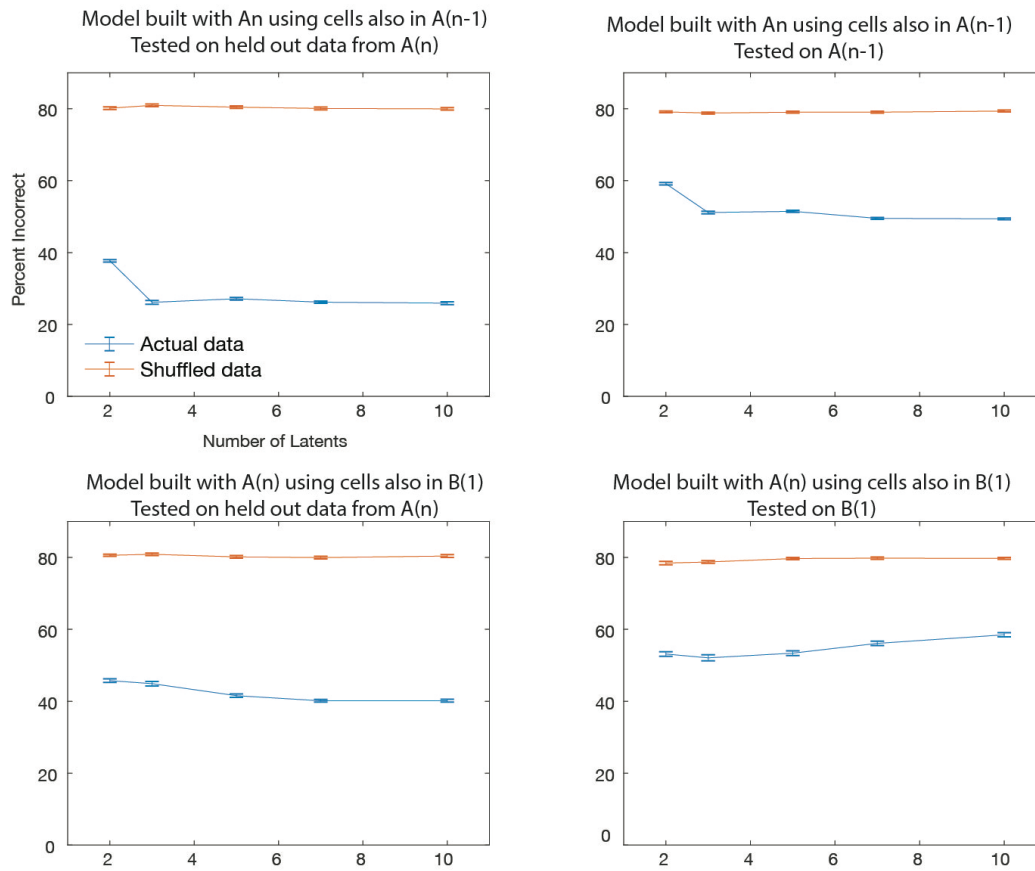


1441

1442 **Figure S11. CSUS2 decoding accuracy with increasing number of latents (Rat 3).**

1443 Percent of incorrect decoding for the CSUS2 model as the number of latents increases. Left
1444 panels: model trained on data from A(n), tested on held out data from A(n). As the number of
1445 latents increases, the model's ability to decode a different session within the same environment
1446 remains stable or slightly decreases. Right panels: model trained on data from A(n), tested on
1447 A(n-1) (top) or B(1) (bottom). Performance remains stable for a different session in the same
1448 environment (upper right panel) but deteriorates with increasing number of latents when the
1449 model is tested in a different environment (lower right panel). Each model was run 100 times.

Figure S12



1450

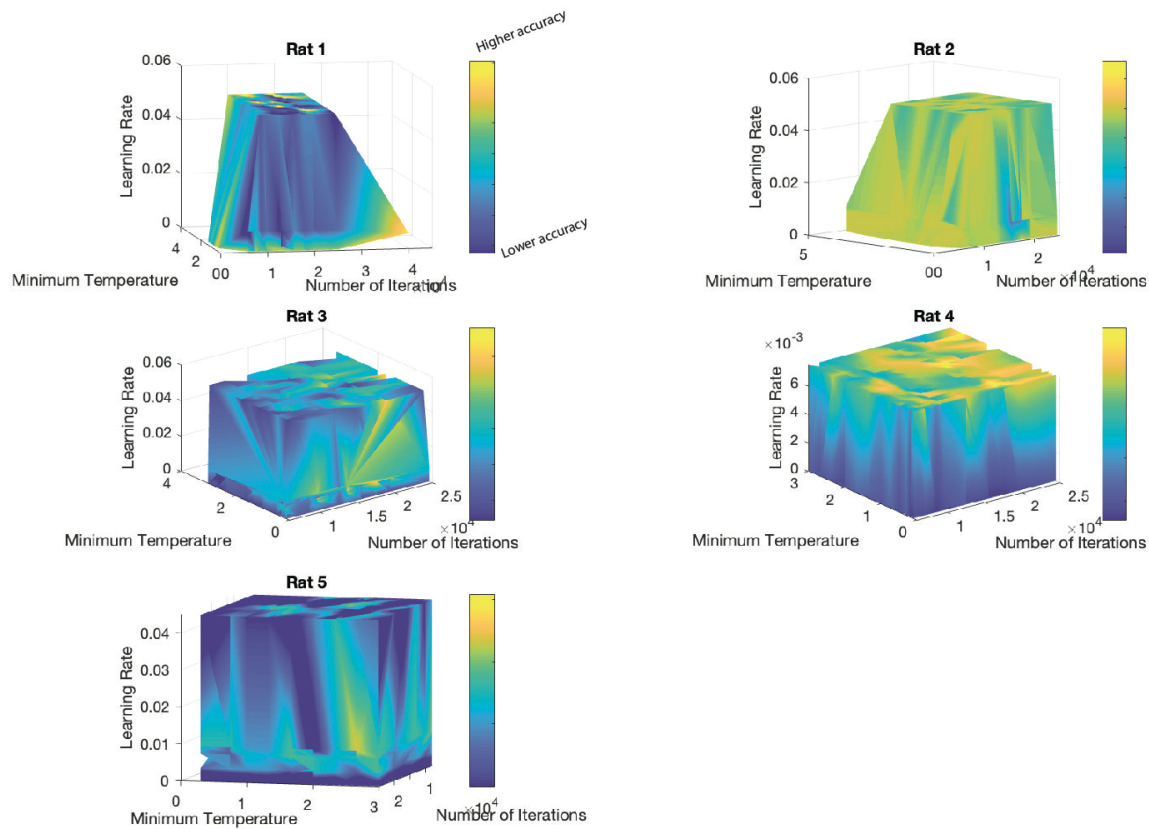
1451 **Figure S12. CSUS5 decoding accuracy with increasing number of latents (Rat 5).**

1452 Same as Figure S11, but for CSUS5; the conditioning period has been divided into five time bins
1453 instead of two. The percent of incorrect decoding is shown as the number of latents increases.

1454 Left panels: model trained on data from $A(n)$, tested on held out data from $A(n)$. As the number
1455 of latents increases, the model's ability to decode a different session within the same environment
1456 remains stable or slightly increases. Right panels: model trained on data from $A(n)$, tested on
1457 $A(n-1)$ (top) or $B(1)$ (bottom). Performance remains stable for a different session in the same
1458 environment (upper right panel) but deteriorates with increasing number of latents when the
1459 model is tested in a different environment (lower right panel). Each model was run 100 times.

1460

Figure S13



1461

1462 **Figure S13. Grid search over decoding parameters for conditioning.**

1463 A grid search was performed over three parameters: minimum temperature, learning rate, and
1464 number of iterations for conditioning decoding. Models were trained using cells from session
1465 A(n) that also appeared in session B(1). The figure shows decoding accuracy for CSUS2 session
1466 B(1) using the models trained on data from session A(n). Yellow areas indicate higher decoding
1467 accuracy. For Rats 1 and 4, the 'Euclidean' distance with 'constant' temperature mode was used.
1468 For Rats 2 and 5, 'cosine' distance with 'constant' temperature mode was used. For Rat 3, 'cosine'
1469 distance with 'auto' temperature mode was used.

1470

1471

1472

1473 **Methods References**

1474

- 1475 1 Wirtshafter, H. S. & Disterhoft, J. F. Place cells are nonrandomly clustered by field
1476 location in CA1 hippocampus. *Hippocampus* **33**, 65-84 (2023).
1477 <https://doi.org/10.1002/hipo.23489>
- 1478 2 Wirtshafter, H. S. & Disterhoft, J. F. In Vivo Multi-Day Calcium Imaging of CA1
1479 Hippocampus in Freely Moving Rats Reveals a High Preponderance of Place Cells with
1480 Consistent Place Fields. *J Neurosci* (2022). [https://doi.org/doi:10.1523/JNEUROSCI.1750-](https://doi.org/doi:10.1523/JNEUROSCI.1750-21.2022)
1481 [21.2022](https://doi.org/doi:10.1523/JNEUROSCI.1750-21.2022)
- 1482 3 Weiss, C. & Thompson, R. F. The effects of age on eyeblink conditioning in the freely
1483 moving Fischer-344 rat. *Neurobiol Aging* **12**, 249-254 (1991).
1484 [https://doi.org/10.1016/0197-4580\(91\)90105-s](https://doi.org/10.1016/0197-4580(91)90105-s)
- 1485 4 Skelton, R. W. Bilateral cerebellar lesions disrupt conditioned eyelid responses in
1486 unrestrained rats. *Behav Neurosci* **102**, 586-590 (1988). [https://doi.org/10.1037//0735-](https://doi.org/10.1037//0735-7044.102.4.586)
1487 [7044.102.4.586](https://doi.org/10.1037//0735-7044.102.4.586)
- 1488 5 Aharoni, D., Khakh, B. S., Silva, A. J. & Golshani, P. All the light that we can see: a new
1489 era in miniaturized microscopy. *Nat Methods* **16**, 11-13 (2019).
1490 <https://doi.org/10.1038/s41592-018-0266-x>
- 1491 6 Silva, A. J. Miniaturized two-photon microscope: seeing clearer and deeper into the
1492 brain. *Light: Science & Applications* **6**, e17104-e17104 (2017).
- 1493 7 Mathis, A. *et al.* DeepLabCut: markerless pose estimation of user-defined body parts
1494 with deep learning. *Nature neuroscience* **21**, 1281-1289 (2018).
- 1495 8 Corder, G. *et al.* An amygdalar neural ensemble that encodes the unpleasantness of
1496 pain. *Science* **363**, 276-281 (2019). <https://doi.org/10.1126/science.aap8586>
- 1497 9 Thevenaz, P., Ruttimann, U. E. & Unser, M. A pyramid approach to subpixel registration
1498 based on intensity. *IEEE Trans Image Process* **7**, 27-41 (1998).
1499 <https://doi.org/10.1109/83.650848>
- 1500 10 Zhou, P. *et al.* Efficient and accurate extraction of in vivo calcium signals from
1501 microendoscopic video data. *eLife* **7** (2018). <https://doi.org/10.7554/eLife.28728>
- 1502 11 CIAtah: a software package for analyzing one- and two-photon calcium imaging
1503 datasets. v. v1.0.0 (Zenodo, 2018).
- 1504 12 Kinsky, N. R., Sullivan, D. W., Mau, W., Hasselmo, M. E. & Eichenbaum, H. B.
1505 Hippocampal Place Fields Maintain a Coherent and Flexible Map across Long Timescales.
1506 *Current biology : CB* **28**, 3578-3588 e3576 (2018).
1507 <https://doi.org/10.1016/j.cub.2018.09.037>
- 1508 13 Olypher, A. V., Lansky, P., Muller, R. U. & Fenton, A. A. Quantifying location-specific
1509 information in the discharge of rat hippocampal place cells. *J Neurosci Methods* **127**,
1510 123-135 (2003). [https://doi.org/10.1016/s0165-0270\(03\)00123-7](https://doi.org/10.1016/s0165-0270(03)00123-7)
- 1511 14 Pearson, K. LIII. On lines and planes of closest fit to systems of points in space. *The*
1512 *London, Edinburgh, and Dublin philosophical magazine and journal of science* **2**, 559-572
1513 (1901).
- 1514 15 Nieh, E. H. *et al.* Geometry of abstract learned knowledge in the hippocampus. *Nature*
1515 **595**, 80-84 (2021).

- 1516 16 Ans, B., Hérault, J. & Jutten, C. Architectures neuromimétiques adaptatives: Détection
1517 de primitives. *Proceedings of Cognitiva* **85**, 593-597 (1985).
- 1518 17 Tenenbaum, J. B., Silva, V. d. & Langford, J. C. A global geometric framework for
1519 nonlinear dimensionality reduction. *science* **290**, 2319-2323 (2000).
- 1520 18 Low, R. J., Lewallen, S., Aronov, D., Nevers, R. & Tank, D. W. Probing variability in a
1521 cognitive map using manifold inference from neural dynamics. *BioRxiv*, 418939 (2018).
- 1522 19 Schneider, S., Lee, J. H. & Mathis, M. W. Learnable latent embeddings for joint
1523 behavioural and neural analysis. *Nature* **617**, 360-368 (2023).
1524 [https://doi.org:10.1038/s41586-023-06031-6](https://doi.org/10.1038/s41586-023-06031-6)
- 1525 20 Pedregosa, F. *et al.* Scikit-learn: Machine learning in Python. *the Journal of machine*
1526 *Learning research* **12**, 2825-2830 (2011).
1527